X-660-74-298
PREPRINT
NASA TM X-70770

THE VARIATION OF SOLAR PROTON ENERGY SPECTRA AND SIZE DISTRIBUTION WITH HELIOLONGITUDE

M. A. I. VAN HOLLEBEKE
L. S. MA SUNG
F. B. McDONALD

SEPTEMBER 1974

GODDARD SPACE FLIGHT CENTER
GREENBELT, MARYLAND

"This paper presents the views of the author(s), and does not necessarily reflect the views of the Goddard Space Flight Center, or NASA."

For information concerning availability of this document contact:

Technical Information Division, Code 250
Goddard Space Flight Center
Greenbelt, Maryland 20771

(Telephone 301-982-4488)

THE VARIATION OF SOLAR PROTON ENERGY SPECTRA AND SIZE DISTRIBUTION WITH HELIOLONGITUDE

M. A. I. Van Hollebeke*

L. S. Ma Sung*

F. B. McDonald

NASA/Goddard Space Flight Center
Greenbelt, Maryland 20771 U.S. A.

*Also: Department of Physics and Astronomy
University of Maryland
College Park, Maryland

ABSTRACT

A statistical study of the initial phases of 185 solar particle events has been carried out using the data from the Goddard cosmic ray experiments on IMPS IV and V. Special emphasis is placed on the identification of the associated solar flare. The parent flare can be determined for 68% of the events. It appears probable that most of the unidentified increases occur on the non-visible disc of the sun. The existence of a "preferred-connection" longitude between 20°W and 80°W is established by examining the heliolongitude of all the flare associated events. It is demonstrated that the energy spectra determined at the time of maximum particle intensity in the 20-80 or 4-20 MeV interval give results identical to that obtained by the "distance-travelled" method of Bryant et al. (1965) and is more generally applicable. A power law in differential kinetic energy appears to give the best representation. It is argued that for heliolongitudes $\lambda_{\odot}$ = 20-80° W, γ_p, the spectral index determined at the time of maximum particle intensity is representative of the source spectra. For these heliolongitudes γ_p displays a surprisingly small range with magnitudes varying mainly between 2.0 and 3.1. At lower energies γ_p is smaller. Previous electron measurements provide almost identical average values of the source spectra over similar energy ranges. These results are discussed briefly in terms of Fermi acceleration models.

For flare events located further away from the nominal field line connecting the earth and the sun, γ_p becomes progressively steeper. The lower energies (4-20 MeV) do not exhibit this behavior. It is argued

that this spectral steepening at the higher energies is the result of energy-dependent escape during the coronal diffusion process. The size distribution can be represented by a power law of the form $dN/dI = I^{-\alpha}$ where N is the number of events per unit intensity and I is the maximum particle intensity at a given energy (usually taken at 40 MeV) with $\alpha \approx 1.15 \pm .1$. The same value of α applies to both eastern and western hemisphere events. The event size, on the average, appears to decrease approximately two orders of magnitude for each 60° away from the preferred connection region.

INTRODUCTION

The basic properties of a solar cosmic ray event observed at 1 AU are determined not only by the size of the event at the Sun, but also by the magnetic configuration of the active region and the solar corona and by the state of the interplanetary medium. All of these quantities display a high degree of variability which results in the great diversity shown by solar particle events. It is clear from recent reviews (McCracken and Rao, 1970; Lanzerotti, 1972; Simnett, 1974; Lin, 1974; McDonald and Fichtel, 1974) that significant progress has been made in the area of interplanetary propagation and in understanding the characteristics of the electromagnetic phenomena associated with particle-accelerating flares. However, there remains considerable uncertainty on the physical processes occurring near the sun.

One approach to understanding both the variability in the production process and coronal diffusion is by a statistical study of the initial phases of a large number of solar particle events. Such a sample is provided by the Goddard Cosmic Ray Experiments on IMPs IV and V. These observations span the period of maximum solar activity during cycle 20. In this paper we describe the procedures for identifying the parent flare of an event and summarize the properties of the 125 events in which the location of the initiating flare could be established. The most important characteristics were found to be: (1) the differential energy spectra measured at the time of maximum particle intensity and (2) the maximum particle intensity at a given energy. By studying the variation of these parameters with the heliolongitude of the

flare, this statistical study establishes the existence of a "preferred connection region" which is centered about the interplanetary magnetic field line connecting the observer to the location of the flare site. For an observer at the Earth, this region extends from 20° W to 80° W. From the study of solar particle events associated with flares in this particular range of longitude, the properties of the particle distribution at the source region can be deduced. Of special interest are the energy spectra at the source and the size distribution of these events.

The energy spectrum at the time of maximum particle intensity is examined in section IV. Over the energy region 20-80 MeV the best representation appears to be a power law in kinetic energy. Characteristic examples of this spectral index, γ_p, are shown along with representations in the form of exponential rigidity. The difference between these two forms of spectra are significant only when the energy range is extended below 25 MeV or when the precision of the measurement is especially good.

The spectral index, γ_p, determined at the time of maximum particle intensity in the 20-80 MeV energy range, shows a strong variation with the longitude of the parent flare. However, for particle events with flare locations between 20°and 80° W, it is found that γ_p exhibits an unexpectedly small variation from event to event with 88% having γ_p between 2.0 and 3.1. At lower energies (< 20 MeV) there is no systematic variation of γ_p with flare longitude. The existence of a characterictic energy spectrum should place considerable restraints on the nature of

the acceleration process. The variation of γ_p with heliolongitude provides information on coronal diffusion. These implications are discussed in section VII.

The size spectrum is analyzed in section VIII. It is shown that the number, N, of proton events, with maximum particle intensity, I, can be described adequately by $dN/dI \sim I^{-\alpha}$, where α is typically $1.15 \pm .10$. A plot of the dependence of peak particle intensity at 20-80 MeV upon solar longitude suggests that the peak intensity falls off by about two orders of magnitude for each 60° of solar longitude in agreement with the earlier results of McCracken et al.,(1967). The interpretation of this intensity variation with longitude is consistent with the corresponding variations of γ_p.

II. DATA ANALYSIS

The data used in this study were obtained from the GSFC Cosmic Ray Experiments aboard the high eccentric earth orbiting satellites IMPS IV and V. These cover a period of five years between May 1967 and Dec. 1972 with short interruptions from May to June 1969 and between November 1971 and February 1972.

The experiment consists of two dE/dX vs. E telescopes; a low energy detector (LED) which detects protons and alpha particles between 4 and 20 MeV/nucleon; and a medium energy detector (MED) which detects particles between 20-80 MeV/nucleon (Bryant et al., 1962; Kinsey, J. H., 1970; and Van Hollebeke et al., 1974). Both of these ranges of particle energies are pulse height analyzed and are free of any background or electron contamination. The thin dE/dX element, MED A, was used to

detect electrons in the .5-1.1 MeV energy range. This element has a geometric factor of 60 cm^2-ster.

The axis of the MED is parallel to the spacecraft spin axis which is stabilized normal to the ecliptic plane. The LED view direction is normal to the spacecraft spin axis with a field of view of $< 20°$. Since the satellite spin rate is approximately 23 rpm, the rate accumulation time of 4.48 seconds is long enough to represent the average intensity in the field of view over all azimuthal directions.

Over the entire observing period some 185 solar cosmic ray events were detected and time histories of those have been described in a catalogue of solar cosmic ray events IMPs IV and V (May 1967-Dec. 1972) (M. A. I. Van Hollebeke, J. R. Wang and F. B. McDonald, 1974). For these events it was required that the proton flux at energies greater than 20 MeV exceed 10^{-4} particles/cm^2-sec-ster-MeV. By demanding a measurable flux above 20 MeV, a better separation from co-rotating events is achieved.

III. FLARE IDENTIFICATION

A. Problems of Identification: The onset time of the 0.5-1.1 MeV electrons were used to identify the associated flare. These electrons travel with a velocity v which is essentially equal to the velocity of light and provide the earliest indication that an event has started. The closest possible flare to this electron onset time (or 20-80 MeV proton onset time when the electron increase was below threshold) that also displayed x-ray and radio emission was chosen as the parent flare. The x-ray data was obtained from the University of Iowa experiments on

Explorer 33 and 35 and from the NRL data on Solrad 9. The radio emissions considered are type II, III and IV or intensive microwave radio bursts. All radio and optical flares data were taken from the N.O.A.A. Solar-Geophysical Data Reports or the I.A.U. Quarterly Bulletin on Solar Activity. As indicated previously it was also required that the > 20 MeV proton flux must exceed 10^{-4} particles/cm^2-sec-ster-MeV.

Over the 52 months of observing, a total of 185 solar particle events were detected. It was possible to identify the parent flare for 125 of these events. This set of 125 events forms the statistical sample on which the present study is based. The corresponding solar and particle data are summarized in Table I. Included are the electron and flare onset times, the flare location and the associated x-ray and radio data.

For several large particle events, there was no association with an optical flare, but the presence of either an intense X-ray, a radio burst or both suggested a possible association with a flare site located behind the visible limb. This is not unexpected since an intense X-ray or radio burst can sometimes be seen 40° behind the limb. Many of these associations have been discussed in the literature and references to those have been made in the table. Of course, the heliocentric longitude of the parent flare could be estimated only if the suspected active region happened to give large flares in the previous or in the next solar rotation. The identification was further strengthened when the proton event was also recorded by another satellite at 1 AU located at large distances from the earth; for example, Pioneer 6, 7, 8, or 9. In total,

8 backside particle events have been identified. For these events, the Hα onset could not be observed so the time of either the X-ray bursts or the type II or IV radio bursts was used. As will be discussed later, most of the remaining 33% of the events that could not be identified with a parent flare represent the contribution expected from flares on the non-visible disc of the sun.

Approximately 75% of those identified events are accompanied by a type II or a type IV radio burst; this is indicated by a cross in the corresponding column in Table I. Some 13% were associated with both a microwave burst and a type III in metric and decametric wavelength and are generally micro-events as discussed elsewhere (F. B. McDonald and M. A. Van Hollebeke, 1973). Some 8% have only a strong centimeter radio burst at the time of the Hα and X-ray maximum. In the last two cases it is expected that a type II or IV radio burst might have been detected with more sensitive instrumentation. Also indicated in the table are those events during which either optical, radio, or X-ray observations were not being made.

The assignment of an initiating flare is partially subjective. In a future paper dealing with the properties of the associated solar events, we will undertake a more quantitative error analysis. At this time we believe that no more than 10% of the events in Table I could be mis-identified.

B. The heliocentric distribution of the flare-associated events: Figure I gives the distribution of those ~125 identified solar events with respect to the heliolongitude of the associated flare. The probability has been normalized to 100 at the maximum of the distribution

and the heliolongitude is taken with respect to the central meridian. Each interval is 30° wide and it can be seen that the probability of observing an event is much larger for flares located between 30° and 60° W longitude and that the probability decreases rapidly outside this range. The sharp drop at 90° W is due to the fact that even moderate sized solar X-ray or radio bursts are generally not detected behind the limb. In other words, particle events originating behind the west limb are detected but the parent flare could not be identified. The data in Figure 1 also suggests that the probability distribution for the visible disc of the sun is symmetrical about 45 $\pm$ 15°W. It is expected this symmetry will be maintained so that the probability distribution between 90°W and 180°W will be the same as between 0 and 90°E. Thus, approximately 38 events will originate between 90°W and 180°W with 8 of these being identified in Table I. Thus, 30 or half of the unidentified events must originate between 90°W and 180°W. Of the remaining ~30 events, probably half could originate between 90°E and 180° leaving fewer than 10% of the events unaccounted for.

A similar study has been made by McCracken et al., (1970) for events occurring between 1965 and December 1967 using data from Pioneer 6 and 7. They report a pronounced bias toward events originating in the western hemisphere. With this larger data sample it is possible to show that the "preferred connection region" corresponds to those times when the interplanetary magnetic field line connects the flare site and the observer and appears to be symmetric about the average position of this field line.

IV. DETERMINATION OF THE PROTON ENERGY SPECTRUM AT THE SUN

An accurate determination of the solar cosmic ray energy spectra at the flare site will provide information on the nature of the acceleration process. However the measurements are made at 1 AU after the source spectrum has been distorted by the effects of coronal diffusion, interplanetary diffusion and velocity dispersion. During the early phases of the event, these effects are dominant. During the decay phase, the effects due to interplanetary diffusion and adiabatic energy losses become increasingly important. As will be shown in section VI at times longer than 24 hours after the release time, these effects appear to be quite substantial.

One approach to this problem has been to plot the different energy components on the basis of distance travelled after the flare maximum. For some events (Bryant et al., 1965) this gives rise to a common curve and the normalization factors can be used to determine the source spectra. However, as Bryant et al. and others (Barcus, 1969; Lin, 1970; Dilworth et al., 1972; Reinhard and Wibberenz, 1974) have shown, this method is not applicable in all cases. In this paper we show that in the limited energy range of 20-80 MeV, the spectrum determined at the time of the maximum particle intensity in the 20°-80°W longitude range appears to be representative of the particle source spectra. Furthermore, it is shown that this simple technique gives results identical to those obtained by a more rigorous method. The determination of the time of maximum particle intensity is based on an examination of the 20-80 MeV time history for the medium energy data. This corresponds to a time when

the lower energy protons have reached their peak flux while the higher energy particle intensity has not decreased appreciably. This was found to be the case even for the fastest decay times. Depending on the time profile at peak intensity the time interval considered can vary from 45 minutes (in the case of the January 14, 1971 event) to about 6 hours. For two thirds of the events, this time interval was either one or two hours. The time of the maximum particle intensity was ambiguous in some cases when there was more than one maximum in a given event. Whenever the spectrum appeared different at the various possible maxima, it was eliminated from the statistics, otherwise the common spectrum was retained, as in the case of the complex backside event on March 30, 1969.

Listed in column 7 of table I are the times of the maximum particle intensity during which the 20-80 MeV proton energy spectrum was measured. Not all of the 125 particle events could be used to study the energy spectrum at the time of maximum intensity. In addition to technical problems such as passage through the radiation belts, or saturation of the MED during several very intense events, there were interplanetary shocks or large magnetic storms which often disturbed the time history of the events, especially at low energies. Furthermore, for some micro-events the intensity above 30 MeV had a non-negligible galactic component. In all these cases, it was not possible to measure γ_p. There were a few cases, where the maximum of the event was difficult to identify and, since there could have been variations of the spectrum from one suspected time of maximum to another, these events have been eliminated from the

statistics. Whenever the spectral index could not be measured, the reason was indicated in columns 7 and 8 of table I. In total, ~90 of the 125 particle events were used in studying the event source spectrum.. Similar procedures were followed for the low energy detector which covered the 4-20 MeV range.

As noted in section II, the look-direction of the Medium Energy Detector is normal to the ecliptic plane while the Low Energy Detector scans in the ecliptic plane. During the onset phase when particle anisotropies are high, this can introduce serious distortion. However, the field aligned anisotropies decrease with a time constant proportional to $1/vt$ (Fisk & Axford,1969) where v is the particle velocity and t is the time spent by the particle in the interplanetary medium. Rao et al., (1971) concludes that in most of the solar proton events, field-aligned anisotropies are observed up to the time of maximum intensity, beyond which the intensity exhibits an equilibrium type of radial anisotropy. Note that an anisotropy in the ecliptic plane which can be represented as $J(\phi) = J_0 + J_1 \cos(\phi-\phi_A)$ will not introduce any distortion since the detector in the ecliptic plane averages over all values of ϕ and hence measures J_0 which is the same as that measured by the detector with its look-direction normal to the ecliptic plane. Thus, by making the measurements at the time of maximum particle intensity we minimize the effects of both field aligned and equilibrium anisotropies. As will be shown later there are significant differences between the 4-20 and 20-80 MeV proton data. It is our contention that this is due to possible energy dependent acceleration and diffusion processes and not to the different look directions of the two telescopes.

Figures 2 and 3 show 8 representative examples of the 20-80 MeV proton time histories. In each case the time interval is indicated for which the spectral index, γ_p, at maximum particle intensity was determined. The 3 events in figure 2 have a classical time history with a relatively short rise time and a well defined maximum. The events in figure 3 include both micro-events and events with more complex time histories. Time-histories of .5-1.1 MeV electrons and lower energy protons are also shown. The latter are of importance in this study only to distinguish any non-velocity-dependent effects. Note also the time delay between the maximum intensity of the 20-80 MeV proton and that of the 6-19 MeV proton. This difference varies from event to event. For some events the time of maximum intensity for the 6-19 MeV protons was close to that of the 20-80 MeV protons. In this case the spectral determination could be made during the same time interval from 6 MeV to 80 MeV; two such examples are given in figure 4. In the case of April 22, 1971, a differential energy power law fits the data from 4 to 80 MeV. For the event on April 20, 1971, there is a knee in the spectrum between 15 and 25 MeV. It is not clear from the data above whether the knee has a real physical meaning from which the energy change process can be deduced (S. S. Muray et al., 1972) or if it is simply an effect of anisotropies which are directed out of the ecliptic plane.

The distance-travelled-method is based on the fact that for some events, the interplanetary diffusion coefficient K is independent of

rigidity and is a function of velocity only, i.e. $K \propto v$. Our ability to define a unique spectrum at the time of maximum particle intensity for the 20-80 MeV protons derives partially from the relatively narrow energy interval and also from the weak energy dependence of the diffusion coefficient. To confirm that this is indeed the case, we have chosen four events when the time interval selected for the spectral determination of γ_p was one hour or less. These are events with the fast decay times where the effects of velocity dispersion should be the greatest. For each of the four examples, the time histories of the three different energy ranges have been used to determine independently the maximum intensity in each of these energy ranges. The energy spectra derived from these three peak intensities are plotted as the dashed diamonds along with the spectral data obtained by the first method (Figure 5). It is seen that in all four cases the two methods give essentially identical results over the 20-80 MeV region. Because the first method is better for small events and for those events with some structure at the peak time, we have consistently used it for all cases.

To insure that anisotropy effects are not important at the time of maximum particle intensity, a detailed comparison was carried out with an essentially identical detector on OGO V. This detector is always looking in the ecliptic plane, pointing in a direction away from the earth and measuring proton intensity in roughly the same energy range. These detector experiments are described in detail by Jones et al., (1967). It was found that near maximum particle intensity the differences

in intensity of the 20-80 MeV protons from both telescopes were small and that the differences in spectral shapes were negligible. Figure 6 shows, for comparison, the spectra of two events at the time of maximum particle intensity. For the event on November 24, 1969, the difference in intensity was roughly 22%, but the spectra had the same slope. For the event on April 22, 1971, the intensity differed by less than 10% and the measured slopes were identical. The first case suggests that although a small variable anisotropy might still be present at this time, it clearly did not affect the energy distribution of the particles. Note also that in April, 1971, the OGO detector was looking in the direction of the nominal field line while in November, 1969, it was pointing in the direction ~60° E from the sun-earth line. Late in an event, when the expected anisotropy is small, the particle intensity detected by OGO V agrees perfectly with those from IMP IV or IMP V.

It has been previously shown that depending on the event or the energy range, the number spectrum can be represented either as a power law in kinetic energy or in the form of exponential rigidity. For example, Freier and Webber (1963) found for 16 large events, the best spectral shape was of the form $J = J_o(t)\, e^{-P/P_o(t)}$, where P is the particle rigidity, and $P_o(t)$ and $J_o(t)$ are functions of time. Generally these spectral determinations were made after the maximum of particle intensity at a time when the decay phase may have been well advanced. In addition, they were concerned with larger events and higher energies than those of this study.

In this experiment, the range of energy generally considered (20-80 MeV) is too small to show a significant difference between a differential energy spectrum and an exponential in rigidity, especially for small events where the uncertainty can be as high as $\pm$ 25% for the higher energy bin. However, whenever a unique spectrum could be determined over an energy range from 10 MeV to 80 MeV, the differential energy spectrum gave a better fit in this energy range than any other representation such as exponential rigidity. This is shown in figure 7 for 3 events with different spectral slopes. The fit in exponential rigidity of the March 26, 1970 data was bad at low energies whereas a differential energy power law spectrum was an excellent fit from 10 to 80 MeV as shown in the first spectrum of figure 8. In addition, some 19 other typical spectra of the ~90 events listed in table I are shown in figure 8. The time history of several of them were included in figures 2 and 3. There are micro-events such as July 30, 1967 and January 14, 1971 for which the higher energy bin is almost equal to the galactic intensity in this energy bin. There are small and medium size events with different spectral indices as well as large size events such as September 1, 1971. For all of these, a differential energy power law spectrum of the form $dJ/dE \sim E^{-\gamma}$, gives a good fit in the 20-80 MeV range.

Column 8 in Table I lists the values of the spectral index γ_p, for the 20-80 MeV protons. The data for the 4-20 MeV protons have not been included in this table. Frequently there were difficulties in obtaining γ_p in this energy interval. It may be that in going from the 20-80 MeV to the 4-20 MeV range, the interplanetary diffusion coefficient K enters a different regime where the energy dependence of K becomes more pronounced. For example, the interplanetary irregularities affect the low energy particles more than the medium energy ones. Some of these irregularities are not only due to shocks but can also be local disturbances in the interplanetary medium. Thus, each time a storm was detected at the earth or any disturbance appears simultaneously in the ~1 MeV and the 4-20 MeV proton intensities, the corresponding 4-20 MeV event was eliminated from the statistics.

Figure 9 gives the distribution of the spectral index γ_p for the two different energy ranges. The curve fits a Poisson like distribution with an average of 2.9 for the 20-80 MeV protons and a harder 2.5 average spectrum for the 4-20 MeV protons. These distributions confirm that, on the average, the spectrum is flatter at lower energies (McKibben, 1972). This data in figure 9 clearly shows that γ_p in general cannot be represented by a single power law over the energy interval 4-80 MeV even when velocity dispersion is taken into account. Note that those distributions represent an average of all flare associated events independent of the position of the parented flare.

V. VARIATION OF THE SPECTRAL INDEX γ_p WITH THE ASSOCIATED FLARE HELIOCENTRIC LONGITUDE

The variation of the spectral index, γ_p, with heliolongitude for 20-80 MeV protons is shown in Figure 10. The γ_p values identified by open circles refer to the 8 "long-rise-time" events in which the maximum in the particle intensity occured more than 24 hours after the onset of the associated flare (c.f. column 8, table I). It is felt that the γ_p measured for these events will have been significantly distorted by interplanetary adiabatic deceleration and coronal diffusion. All other events show a definite increase in γ_p with increasing longitude away from the preferred connection region. This pattern is shown by the dashed contour lines which enclose more than 92% of the data points. For many of those cases lying outside the dashed contour line it is often possible to identify features such as interplanetary shocks close to the observer or multiple structure over the period of peak intensity that contributed to the anomalous value of the rise time. The solid line is the resulting least square fit obtained for those events within the contour lines. This distribution has a well defined minimum for events associated with flares between $\lambda_\odot$ = 20° and 80° W. Furthermore, in this region the dispersion in γ_p is surprisingly small with 88% of the 32 events having γ_p between 2.0 and 3.2 (Fig. 11).

Moving away from the 50° $\pm$ 30° W region, γ_p can be represented approximately by:

$$\gamma_p\ (\lambda_\odot) = 2.7\ \ [1 + \Delta\lambda/2\ ]$$

Where $\Delta\lambda$ is the separation angle in radians between the flare longitude and 50° W. As previously emphasized, coronal and interplanetary conditions are continuously changing so the dispersion displayed in Fig. 10 is not unexpected. There were no systematic variations of γ_p with heliocentric longitude for the 4-20 MeV data (Fig. 12).

VI. SOURCE SPECTRA AND THE ACCELERATION PROCESS

For the preferred connection region, $\lambda_{\odot}$ = 20-80° W, coronal diffusion effects should be at a minimum and the variations observed in γ_p from event to event are principally variations in the source spectrum itself. However, it is first necessary to establish that interplanetary diffusion and the resulting adiabatic energy losses are small during the initial phase of an event.

Many studies have shown for both electrons and protons over a wide span of energies that the onset time and the rise time are minimum for an observer close to the interplanetary field line which connects to the flare region. (Barouch et al., 1971; Simnett, 1971; Datlowe, 1971; McKibben, 1972; and Reinhard and Weibberenz, 1974). For example, in the present data this can be observed in the plot of the difference between the 20-80 MeV proton onset time and the time of maximum intensity as a function of heliolongitude (Fig. 13). All of these results clearly establish that during the early phases of an event, the propagation process is most efficient for an observer near the earth when the solar flare is located between $\sim \lambda_{\odot}$ = 20° and 80°W.

It is expected that solar cosmic rays will lose energy in the interplanetary medium as they are scattered in the magnetic irregularities moving with the solar wind (Parker, 1965; Gleeson and Axford, 1967). The amount of this energy loss or adiabatic deceleration will be a function of the particle diffusion coefficient. Axford (1970) has suggested that the importance of convection and energy loss processes relative to diffusion can be obtained from the expression for particle streaming

$$S(r, t) = C\ V\ U - K(r) \frac{\partial u}{\partial r}(r,t)$$

where V is the solar wind velocity, U (r,t) is the particle density at a given energy E, C = 2/3 (1 + γ) is the Compton-Getting factor for non-relativistic particles and K is assumed to be of the form

$$K(r) = K_0\ r^b$$

The significance of the convective and diffusive effects can be estimated by examining the ratio, D, of the two terms

$$D = \frac{CVU}{K(r)} \left(\frac{\partial U}{\partial r}\right)^{-1} = \frac{(2-b)CVt}{r}$$

Assuming b = 1/2 gives
D = .035 t for V = 400 km/sec where t is in hours.

At ~29 hours convective and diffusion effects will be equal. The median rise time T_r (between particle acceleration and maximum particle intensity at 1 AU) for the 32 events between 20 and 80° W is 4.5 hours (Figure 14) and convection effects would be expected to be on the order of 10%. This is borne out by the more detailed computation of Palmer (1973) showing that for b = 1/2 the energy loss (for T_r = 5.2 hours) will be 12% which is in excellent agreement with the estimate. For T_r = 10 hours, the calculated energy loss will have increased to 25% of the original energy. However, only 12% of the events have $T_r > 6$ hours (Figure 14). The largest variation of K as a function of energy that has been assumed is for $K \propto \beta\ R^{1/2}$ which would imply that K could vary by a factor of 3 from 20 to 80 MeV. (Our spectral results indicate, however, a much weaker rigidity dependence). From the calculations of Palmer (1973) it can be estimated that for T_r = 5 hours, the energy loss will increase from

12% to 20% if κ is decreased by a factor of 3. For a rise time of 10 hours, these will change from 25% to 35% for similar changes in κ. These estimates for two different rise times both suggest that the most extreme variations in κ as a function of energy would result in a 10% shift between 20 and 80 MeV. Most estimates of the variation of κ with energy are smaller than the extreme case we have chosen and resulting spectral distortions are smaller.

Figure 15 shows the distribution of the rise time T_r as a function of the spectral slope γ_p for events associated with longitude 20° W to 80° W. There is a tendency for a long time delay to be associated with a smaller value of γ_p, in agreement with the predicted effects of adiabatic deceleration in the interplanetary medium.

From the previous discussion it is clear that for flares with $\lambda_\odot$ between 20° and 80° W, γ_p should be representative of the injection spectrum with $dJ/dE = C\ E^{-2.7}$ over the 20-80 MeV range. It is customary to express the source spectra in terms of $N(E) \propto E^{-\delta_o}$ where N(E) is the number of particles with kinetic energy E per unit volume

$$N(E) \propto \frac{1}{V}\frac{dJ}{dE} \propto \frac{1}{E^{\frac{1}{2}}}\ \frac{dJ}{dE} \propto C\ E^{-3.2}$$

for 20-80 MeV proton energies. For lower energies $\gamma_p = 2.4$ and $\delta_o = 2.9$ where $\delta_o = \gamma_p + 0.5$ for non-relativistic particles. As emphasized previously, γ_p displays a relatively small variation with 88% of the events having values between 2.0 and 3.2 while the peak intensity varies over some 4 orders of magnitude. There is some suggestion in the data

of an inverse correlation between the peak intensity and γ_p. The largest event during which the MED did not saturate (February 25, 1969) also had the smallest value of $\gamma_p = 1.3 \pm .2$.

There is a remarkable similarity between the median value of γ_p reported here for protons and the values previously reported for electrons of approximately the same energy. Using the Goddard cosmic ray data from IMP IV, Simnett (1972) found a spectral index $\gamma_e = 3.0 \pm 0.2$ for 3-12 MeV electrons. Note that over this energy range the electron velocity is close to c so $\delta_e = \gamma_e$. For the 12-45 MeV region Datlowe (1971) reported a median value of $\gamma_e = 3.5$. This suggests that the average source spectrum is similar for protons and electrons of the same energy.

A number of models for solar particle acceleration have been proposed. Wentzel (1965) has shown that by varying the conditions for particle escape from the acceleration region, the basic Fermi process can be used to produce spectral shapes ranging from exponential energy, exponential rigidity to power laws either in rigidity or energy. A more detailed model in which the particles are accelerated in a perpendicular MHD shock with a stochastic scattering of the particles in the magnetic field irregularities has been shown by Schatzmann (1963) to predict power law spectra in reasonable agreement with that reported here. Friedman and Hamberger (1969) calculated that acceleration at a neutral sheet could produce the proper spectral forms. There are two examples of a large number of processes that have been proposed (c.f. Syrovatskii, 1969). It is not evident that these can be modified to

produce similar spectral shapes for both electrons and protons. A number of other observational parameters are needed to help define a proper model. These parameters include the relative numbers of electrons, protons and alpha particles accelerated to a given energy as well as better definitions of coronal conditions. The additional particle measurements will be presented in a later paper.

There is an obvious difference between the 20-80 MeV proton spectrum and the 4-20 MeV spectrum. This indicates either a break in the source-spectrum, different propagation conditions, or both. It is expected that the low energy spectrum should be more distorted by propagation effects in the interplanetary medium. It has also been shown (Feit, 1973; McKibben, 1973) that there is often storage and continuous ejection for low-energy particles. The energy degradation of the spectrum has been shown by Krimigis and Verzariu (1971), who estimated from observation of the solar flare proton spectrum around 1 MeV, that a storage of ~10 hours could take place for some events in a region of the corona with density $\simeq 10^5$ cm^{-3}. Even with these uncertainties on the propagation conditions at low energy, it appears most probable that part of the spectral change is produced at the source. A two-step acceleration process with a knee around 10 MeV, as suggested by Sturrock (1973), does not seem incompatible with the previous results.

VII. THE SOFTENING OF γ_p WITH INCREASING DISTANCE AWAY FROM THE PREFERENTIAL LONGITUDE: INTERPRETATION

It was found in section V, that the 20-80 MeV proton spectrum, as well as a number of other observable properties of the solar particle events, varied with the longitude of the parent solar flare. The proton spectrum associated with flares at a longitude $\Delta\lambda$ radian away from the observer's "preferential longitude", $\lambda_\odot$, can be expressed approximately as

$$\frac{dJ}{dE} \propto E^{-\gamma_{p_o}\left(1 + \frac{|\Delta\lambda|}{2}\right)}$$

where γ_{p_o}, the characteristic source spectra observed for 20-80 MeV protons (see section VI), equals ~2.7, $\lambda_\odot$ corresponds approximately to the helio-longitude of the Archimedes spiral field line at the earth with $\lambda_\odot \cong 50° \pm 30°$ W depending on the velocity of the solar wind. We interpret this variation of the proton energy spectrum with longitude as a coronal propagation effect.

Essentially two models have been proposed for the initial propagation of solar particles:

1) the azimuthal propagation takes place in the interplanetary medium (Burlaga, 1967, and Lupton and Stone, 1973).

2) the azimuthal propagation takes place in the solar corona as suggested by Reid (1964), Axford (1965) and Fan et al. (1968).

A number of papers had discussed these two models in the light of recent observations (McKibben, 1973, Reinhard and Wibberentz, 1974). The experimental evidence suggested that the azimuthal particle distribution must occur near the sun. For example the anisotropy at early times is generally aligned with the interplanetary magnetic field and is not dependent on the position of the initiating flare. The initial magnitude of the particle anisotropy is also not dependent on this position (McCracken et al., 1968; Fan et al., 1968; Rao et al., 1971).

Based on these observations we adopt the basic ideas of coronal diffusion as originally proposed by Reid (1964). The particles released by the flare propagate through the solar atmosphere experiencing energy degradation by ionization loss and gradually leaking out into interplanetary space. The particles detected by an observer near the earth are those which made their escape in the solar longitude region which has good field connection with the observer. It is known that energy loss by ionization would affect the low energy particles much more strongly and would result in a flattening of the spectrum. For example, in Englade's (1971) treatment the effect on the 20 MeV proton was about eight times larger than that on the 80 MeV proton. Such a flattening of the spectrum between 20-80 MeV is in strong disagreement with the observation. The effect of ionization loss must be negligible and can be disregarded in this energy range during the initial phase.

Observations on the nature of particle-transport in the corona have found a rather weak energy dependence. Lanzerotti (1973) studied the

time difference between the observed particle onset time and the rectilinear sun-earth travel time as a function of solar longitude using protons in different ranges of energy between .6 MeV and ~25 MeV. These results were interpreted in terms of a diffusive motion in the corona. Lanzerotti concluded that the ratio of the diffusion coefficient to the altitude at which the coronal transport occurs, K_c/R_c^2, was independent of energy. In a more extensive study of the variation of the particle rise time with associated flare longitude for $>$ 10, $>$ 30, and $>$ 60 MeV protons, Reinhard and Wibberenz (1973, 1974) succeeded in separating the effects of coronal propagation and interplanetary propagation and found that the coronal propagation is energy independent. It appears that the transport process in the corona is a combination of coronal drift and coronal diffusion (Reinhard and Roelof, 1973; Reinhard and Wibberenz, 1974).

These studies all indicate that the coronal transport (drift and/or diffusion) should not affect the energy spectrum in the energy range considered here during the rise to maximum intensity. To account for the observed spectral steepening with increasing azimuthal distance from the flare it is necessary to assume that the escape rate from the corona is energy dependent. Note that this loss term should not have a strong influence on the observed onset and maximum times, but rather will affect the intensity (Reid, 1964).

Neglecting the ionization loss, and assuming that coronal diffusion is independent of energy, in agreement with the observations, it is possible to find the energy dependence of the escape rate from the variation of γ_p with $\lambda_\odot$.

For simplicity we shall consider a two dimensional coronal diffusion model. The number density at time t after acceleration and distance ℓ along the diffusive layer from the flare site can be expressed as

$$U(\ell,E,t) = \frac{U_o E^{-\delta_o}}{4\sigma t} \exp\left(-\frac{\ell^2}{4\sigma t} - \eta(E)\, t\right) \qquad (1)$$

In this expression, similar to the solution given by Reid (1964) and Englade (1971), $U_o E^{-\delta_o}$ is the number density spectrum at injection, σ, the coronal diffusion coefficient and $\eta(E)$, the escape rate. Only the escape rate is assumed to be a function of energy.

The rate at which particles escape from the corona at time t and distance ℓ is $\eta(E)U(\ell,E,t)$. Since these particles must propagate in the interplanetary space, the number density detected at 1 AU will be the convolution $\int_o^t \eta(E)\, U(\ell,E,t-u)\, f(u)\, du$ where f(u) describes the effect of the interplanetary propagation. In the coronal transport model it is argued that for events located away from the preferred connection region a large portion of the particle propagation is due to coronal diffusion and/or drift whereas the effect of interplanetary propagation plays a considerably minor role. This implies that f(u) has a relatively narrow profile and in the vicinity of $u \approx o$ where f(u) is appreciable the escaped particle distribution $\eta(E)\, U(\ell,E,t-u)$ is a very slowly varying function of u. Thus the number density observed at 1 AU becomes simply $N(\ell,E,t) = \eta(E)U(\ell,E,t)\, F(t)$ where $F(t) = \int_o^t f(u)\, du$ accounts for the interplanetary effect. Using equation (1) $N(\ell,E,t)$ becomes:

$$N(\ell,E,t) = \frac{U_o}{4\sigma t} F(t) \eta(E) E^{-\delta_o} \exp\left(-\frac{\ell^2}{4\sigma t} - \eta(E)t\right) \qquad (2)$$

Since the density spectral index δ_p is defined as

$$\frac{E}{N}\frac{dN}{dE} = -\delta_p$$

equation (2) becomes

$$\delta_o - \frac{E}{\eta}\frac{d\eta}{dE} + E\frac{d\eta}{dE}t = \delta_p \qquad (3)$$

A relation between the spectral index γ_p and the rise time T_r, between particle acceleration and the maximum particle intensity at 1 AU, is indicated in Figure 16 for 20-80 MeV protons. Two contour lines were drawn to enclose all the data points. It is evident that a linear relation between γ_p and T_r exists of the form

$$\gamma_p = a\,T_r + b_1$$

or $$\delta_p = a\,T_r + b \qquad (4)$$

with $b = b_1 + .5$, where the value of .5 enters since the intensity is proportional to the particle velocity times number density. Substituting (4) into (3) gives

$$\delta_o - \frac{E}{\eta}\frac{d\eta}{dE} + E\frac{d\eta}{dE}T_r = a\,T_r + b \qquad (5)$$

Since neither $\eta(E)$ nor $\frac{d\eta(E)}{dE}$ depends on time, equation (5) can be used to solve for both $\eta(E)$ and $\frac{d\eta}{dE}$ by substituting two different times (T_{r1}, T_{r2}) into (5). The difference at the two different times then gives

$$E\frac{d\eta}{dE}(T_{r1}-T_{r2}) = a\,(T_{r1}-T_{r2})$$

or $$\frac{d\eta}{dE} = \frac{a}{E} \qquad (6)$$

Substituting (6) into (5) gives

$$\eta(E) = \frac{a}{\delta_o - b} \tag{7}$$

In the limited energy range between 20-80 MeV, the values of a and b were approximated by constants. Over a more extended range, it is expected they would be a function of energy. The observed variation of γ_p between the 4-20 and 20-80 MeV interval suggests that the spectral index is energy dependent.

Since from Figure 16 $a \approx (4.5 \pm 2.5)10^{-5}$, $b \approx 2.9$ and the density spectral index δ_o at injection was found to be ~3.2, at a mean energy of $\bar{E} \approx 40$ MeV,

$$\eta(\bar{E}) = \frac{a}{\delta_o - b} = \frac{(4.5 + 2.5)10^{-5}}{3.2 - 2.9} = (1.5 \pm .8)10^{-4} \text{ sec}^{-1}$$

and $\eta(80 \text{ MeV}) - \eta(20 \text{ MeV}) = a \ln (\frac{80}{20})$

$$= (6.2 \pm 3.5)10^{-5} \text{ sec}^{-1}$$

In other words the steepening of the spectral index γ_p can be interpreted by an increase in the loss rate of ~ 35-45% from 20 MeV to 80 MeV. Our estimate of $\eta(\bar{E})$ can be compared with an order of magnitude estimate of the escape rate given by Reid (1964). Using the data of the September 28, 1961 event, he found an upper limit $\eta \simeq 3.5\ 10^{-4}$ sec^{-1} for protons between 130 and 600 MeV.

It is important to emphasize that the calculations above refer to the average changes in $\eta(E)$. It is expected that there will be large local variations depending on the local coronal magnetic configuration (c.f. Altschuler and Newkirk, 1969). These local variations probably account for the anomalous longitude variations observed by a network of satellites during the April 10, 1969 event (McCracken et al., 1971).

If instead of coronal transport, we had assumed an interplanetary propagation model, the particles associated with flares at longitudes away from the "preferred longitude" would be the result of a diffusion across the field lines. Since $K_\perp$, the diffusion coefficient perpendicular to the magnetic field increases with increasing particle velocity, the high energy particles would have better access across the field and therefore a flatter spectrum would result as the azimuthal distance from the flare is increased. This is in disagreement with the present observations. Note that, at late time ($>$ 3 days) McCracken et al., (1971) found a steep spectrum for the particles associated with flares close to the preferred connection region while the spectrum became increasingly flat for particles at larger distances from this region. One explanation may be that the diffusion across the field line is sufficiently small that it can be neglected at early time, but at late times it becomes more important since particles will have a chance to propagate across the field to arrive at the earth. In other words $K_\perp$ is not 0 but is small compared to K_{11}. This would have the effect of depleting the high energy particle population in the flare associated longitude region and thus steepen a spectrum which was flat at early time. On the other hand, the preferential arrival of the high energy particles in a region away from the flare associated longitude would flatten a spectrum which was steep at early time.

In summary, it was shown in this section that a steepening of the spectrum away from the flare longitude connected region can be explained by an energy dependence of the escape rate in the corona. It was

estimated that the escape rate of the 80 MeV protons may be some 35-45% larger than for the 20 MeV protons. This dependence effect may also contribute to a change of intensity with longitude and influence the longitudinal distribution of the number of detected events as discussed in the next section.

VIII. SIZE DISTRIBUTION OF FLARE ASSOCIATED PARTICLE EVENTS

The compilation of IMP IV and V data can be used to study the size distribution of solar particle events. This information as tabulated in Table II and Figure 17 displays the number of events per unit of intensity as a function of intensity for all detected events. To minimize the effect of the spectral dependence upon longitude, the peak proton intensity measured at 40 MeV is used to characterize the size of the event. The galactic background fixes the limit of detectability of event intensity to $\simeq 10^{-4}$ particles/cm^2-sec-ster-MeV above 20 MeV. This is some two orders of magnitude below the threshold in the data used by Reinhard and Roelof (1974) in a more recent report. The size distribution (Figure 17) of all detected particle events can be adequately described by $\frac{dN}{dI} \sim I^{-\alpha}$ where I is the maximum differential intensity, $\frac{dJ}{dE}$ in units of particles/cm^2-sec-ster-MeV and dN, the number of events in the range of intensity dI. α is found to be $1.15 \pm .05$. The size distribution of the flare-identified events is also plotted in Figure 17. Included are all the events listed in Table I. Note that all detected events above 10^{-1} particles/cm^2-sec-ster-MeV have been identified. Note also that the form of the distribution is the same as the one for all detected events and α is constant within the limit of accuracy. This suggests that the probability of identifying an event is approximately the same for the very low intensity and for the medium size intensity events.

Figure 18 shows the longitudinal dependence of the peak intensity (at 40 MeV) of the solar particle events listed in Table I. In Figure 19,

the data has been summed over two longitudinal intervals $\lambda_\odot$ = 20° W - 60° W and $\lambda_\odot$ = 20° E - 60° E. For most of the high intensity events (≥ 2 particles/cm^2-sec-ster-MeV), the MED detector was saturated near the maximum. To compensate for the lack of data for those events, the maximum intensity at 40 MeV was deduced from > 30 MeV and > 60 MeV proton intensity of the APL experiments (Bostrom, et al.).

The intensity distribution (Figure 18) does indicate a maximum of intensity in the 20° - 60° W longitude range and a decrease of one or two orders of magnitude every 60° from the "preferential longitude range" as it was suggested by McCracken et al. (1967) and McCracken and Rao (1970). Furthermore, it is seen in both longitudinal ranges (Figure 19), the form of the distribution is the same as for the total number of events and is expressed as

$$\frac{dN}{dI} = A(\lambda)\ I^{-\alpha} \text{ with } \alpha = \text{const.} = 1.10 \pm .05$$

$A(\lambda)$ is a function of the longitude. For $\lambda_\odot$ = 20°W-60°W, $A(\lambda) = A_{\lambda_o} = 2.7$, and the $\lambda_\odot$ = 60°-20° East, $A(\lambda) = A_{\lambda_1} = 1.1 \pm .05$. The distribution between 20°E and 20°W is intermediate between the two distributions shown in Figure 19. As will be discussed in a future paper, it appears likely that a significant part of the variation of the intensity with longitude is probably due mainly to the variation of the spectral index with longitude as shown in the previous section with the number of events observed at longitude λ above intensity I

$$N = \frac{A(\lambda)}{.10}\ I^{-.10 \pm .05}$$

where $A(\lambda) = A(\lambda_o)\ [C(\lambda)\ E^{-\gamma p_o (\frac{\lambda-\lambda_o}{2})}]^{+ .10 \pm .05}$

$C(\lambda) \leq 1$, an attenuation factor which is a function of longitude, depends on the conditions of propagation in the corona. $\gamma_{p_o} \simeq 2.7$ is the characteristic spectral index. The longitude λ is in radian.

It is expected that different results would be obtained at lower energies where the behavior appears much more complex.

DISCUSSION

It is important to emphasize that this is a statistical study and significant deviations are expected from event to event. Furthermore, all particle increases above a given threshold have been included so this investigation is biased toward small and moderate sized events. Nevertheless, it is surprising how well many of the event parameters are ordered by considering the heliolongitude of the parent flare. The longitudinal variations of the identified events establishes the existence of a preferred connection region that extends from approximately $\lambda_{\odot}$ = 20° W to 80° W. The width of this region is due not only to variations in the solar wind velocity but probably also to the existence of a fast diffusion region in the corona (Reinhard and Wibberenz 1974). We have not separated these two effects in this paper.

The relatively small variation in the source spectra for 20-80 MeV protons for events in the preferred connection region suggests the basic acceleration conditions are not greatly altered from event to event. The fact that solar electrons in the same energy range have spectra similar to that of the protons is unexpected. This requires more detailed study. Of special interest will be the corresponding behavior of the helium nuclei in these events.

The present study further confirms that the processes involving low energy particles are more complex than those involving particles above ~20 MeV. This is probably due to more frequent solar injections and longer storage times at the sun for the lower energy particles.

The variation of γ_p with heliolongitude suggests that particle escape from the corona is energy dependent. A more detailed study of this effect is now underway.

TABLE I - SOLAR FLARE PARTICLE EVENTS (May 1967 - Dec. 1972)

DATE	.5-1.1 MeV ELECTRON ONSET TIME (UT)†	SOLAR FLARE ASSOCIATION					20-80 MeV MAX. TIME* (UT)	20-80 MeV SPECTRAL INDEX γ ($\frac{dJ}{dE} \sim E^{-\gamma}$)
		Hα Time (UT) onset	Max.	X-Rays	Radio Burst cm; Type III	Radio Burst Type II and/or IV	Flare Location	
1967								
May 24	not available	(23)1835	(1845)	yes	yes	X	N 31 E 25	Saturated	---
May 28	0600±0003	0527	(0546)	yes	yes	X	N 22 W 32	0800-1200	2.7±.1
June 06(1)	0603±0006	---		---	---		Reg. 8818~W150	1730±0030	2.5±.1
July 29	MED: P2100±0030	1939	(1948)	yes	yes		N 23 W 21	0230±0030	2.3±.25
July 30	0515±0003	0508	(0512)	yes	yes		N 25 W 26	0070±0015	3.0±.2
July 30	0635±0005	0615	(0625)	yes	yes		N 28 W 30	0745±0015	3.0±.1
July 30	1634±0003	1612	(1635)	yes	yes		N 26 W 36	---	---
July 30	1950±0003	1946	(1955)	yes	yes		N 30 W 33	2130±0030	2.8±.2
Aug. 1	>1500<2200	1722	(1736)	yes	yes	X	N 27 W 62	2330±0030	2.25±.2
Aug. 2	MED: P0845±0015	0757	(0800)	yes	no observation		N 27 W 60	0930±0030	2.7±.2
Aug. 2	1738±0003	1727	(1732)	no observation	yes		N 26 W 76	2130±0030	3.1±.1
Aug. 3	0936±0003	0918	(0927)	yes	yes	no obs.	N 27 W 85	1130±0030	3.0±.2
Nov. 2	0845±0015 1105±0007	0852	(0857)	yes	yes	X	S 18 W 02	1600-1900	3.8±.1
Nov. 4	1212±0005	1151	(1154)	yes	yes	X	S 18 W 33	1430±0030	3.2±.1
Nov. 7	0200±0100	0157	(0159)	yes	---	---	S 15 W 51	0500±0100	2.8±.1
Dec. 3(2)	0915±0005	---		yes ~ 0855	yes	X	Reg. 9091~W105	1430±0030	2.8±.1
Dec. 12	0100±0200	(11)2347	(2358)	yes	yes	X	S 21 W 18	0700-1500	2.3±.1
Dec. 16	0427±0005	0247	(0256)	yes	yes	X	N 26 E 66	undeter.	
Dec. 29	0057±0003	0047	(0050)	yes	yes		S 26 W 77	0145±0015	2.2±.2
1968									
Jan. 11	1730±0030	1659	(1701)	yes	yes	X	S 25 W 39	2300±0200	2.7±.1
Jan. 14	MED: P2115±0015	2006	(2015)	yes	yes	X	N 17 W 42	0230±0030	small I(b)
Feb. 1	1830±0003	1809	(1812)	yes	yes	X	N 17 W 20	2015±0015	" "
Feb. 1	1930±0010	1915	(1920)	yes	yes	X	N 16 W 16	2215±0015	" "
Feb. 2	0550±0003	0541	(0547)	yes	yes	X	N 15 W 23	0645±0015	" "
Feb. 17	0315±0003	0251	(0254)	yes	yes	X	N 17 W 47	0600-0800	2.4±.1
Mar. 21	1610±0020	1422	(1429)	yes	yes	X	N 17 W 54	1800-2200	2.65±.15
Apr. 26	1547±0003	1431	(1437)	yes	yes	uncertain	N 09 W 49	1900±0030	2.3±.1

* This maximum time is the time of measurement of the spectral index γ_p

† MED Proton (20-80 MeV) onset time is used whenever the electron onset time is uncertain.

TABLE I - CONTINUED

DATE	.5-1.1 MeV ELECTRON ONSET TIME (UT)	SOLAR FLARE ASSOCIATION						20-80 MeV MAX. TIME* (UT)	20-80 MeV SPECTRAL INDEX γ ($\frac{dJ}{dE} \sim -E^{-\gamma}$)
		Hα Time (UT) onset	Max.	X-Rays	Radio Burst cm; Type III	Type II and/or IV	Flare Location		
1968									
June 09	0917±0003	0835	(0856)	yes	yes	X	S 14 W 08	1500±0100	3.0±.1
Jul. 06	1510±0010	0946	(0956)	yes	yes	X	N 10 E 90	(07)1800-0600	1.8±.1 (a)
Jul. 09	1900±0030	(08) 1707	(1727)	yes	yes	X	N 13 E 59	(10)1200-2600	2.9±.2 (a)
Jul. 12	0030±0030	0000	(0013)	yes	yes		N 12 E 10	0500-0700	4.0±.1
Jul. 12	1410±0010	1341	(1415)	yes	yes	X	N 11 W 20	(13)0500-0600	5.0±.2
Aug. 14	1400±0010	1326	(1333)	yes	yes	X	N 13 W 80	1830±0030	2.6±.1
Sept.26	0700±0012	0026	(0031)	yes	yes	X	N 14 E 35	1700±0100	4.5±.2
Sept.28	1100±0005	0721	(0808)	yes	yes		S 19 E 39	1830±0030	5.0±.1
Sept.29	0955±0020	0922	(0941)	yes	yes	X	N 13 W 13	undetermined	
Sept.29	1700±0003	1618	(1623)	yes	yes	X	N 17 W 52	2300±0100	2.00±.15
Oct. 04	0040±0003	(03)2348	(2408)	yes	yes	X	S 16 W 37	0600±0030	2.7±.2
Oct. 24	MED:P1000±0200	(23)2356	(2407)	yes	yes	X	S 12 E 59	(25)0900-1500	Low E. Event
Oct. 26	MED:P0430±0030	0046	(0119)	yes	yes		S 20 E 32	1330±0030	3.8±.1
Oct. 27	MED:P1430±0030	1318	(1324)	yes	yes	X	S 17 E 17	2130±0030	3.15±.2
Oct. 29	1547±0005	1114	(1234)	yes	yes	X	S 16 W 12	1930±0030	3.5±.1
Oct. 31	0032±0005	(30)2339	(2413)	yes	yes	X	S 14 W 37	storm cond.	-
Nov. 01	0930±0030	0820	(0905)	yes	yes	X	S 18 W 47	storm cond.	-
Nov. 02	>0900,<1800	0949	(1012)	yes	yes	X	S 14 W 66	perigee	-
Nov. 04	0538±0003	0520	(0542)	yes	yes	X	S 15 W 90	storm cond.	-
Nov. 18	uncertain	1017	(1033)	yes	yes	X	N 21 W 87	saturated	-
Dec. 03	0730±0100	(02)2115	(2119)	yes	yes	X	N 21 E 90	(05)0100±0100 (06)0100±0200	2.5±.2 (a)
Dec. 27	1330±0030	1046	(1056)	yes	yes	X	N 16 E 02	(28)0200±0100	2.6±.2
1969									
Jan. 24	0757±0003	0706	(0728)	yes	yes		N 20 W 09	1000-1200	3.7±.1
Feb. 24	2333±0005	2305	(2315)	yes	yes	X	N 12 W 32	(25)0300±0100	2.6±.1
Feb. 25	0922±0007	0900	(0913)	yes	yes	X	N 13 W 37	1230±0030	1.3±.2
Feb. 26	0500±0012	0418	(0427)	yes	yes	X	N 13 W 46	0830±0030	2.15±.15
Feb. 27	1436±0006	1348	(1413)	yes	yes	X	N 13 W 65	2100-2600	2.0±.25
Mar. 12	MED:P1830±0003	1739	(1742)	yes	yes	X	N 12 W 80	2100±0100	2.1±.1

TABLE I - CONTINUED

DATE	.5-1.1 MeV ELECTRON ONSET TIME (UT)	SOLAR FLARE ASSOCIATION						20-80 MeV MAX. TIME* (UT)	20-80 MeV SPECTRAL INDEX γ ($\frac{dJ}{dE} \sim -E^{-\gamma}$)
		Hα Time (UT) onset Max.	X-Rays	Radio Burst cm; Type III	Radio Burst Type II and/or IV	Flare Location			
1969									
Mar. 21	MED: P0538±0003	0139 (0159)	yes	yes	X	N 19	E 16	1530±0030	3.3±.15
Mar. 27	1440±0010	1323 (1341)	yes	yes	X	N 21	W 68	2330±0030	2.2±.1
Mar. 30(3)	≤0500±0030	<0332	yes~0248	yes	X	N 19	~W 110	0830±0030	2.2±.2
								(31)0600-1200	
Apr. 10	2030±0100	<0410 (0414)	yes~0356	yes	X	N 11	E 90	Saturated	--
**									
1969									
Sept.10	2200±0200	0518 (0522)	yes	yes	X	S 20	E 69	(12)1000-2400	Small I.(b)
Sept.25	0738±0003	0654 (0736)	yes	yes		N 13	W 14	1000-1200	3.5±.2
Sept.27	≤0730	0347 (0412)	yes	yes	X	N 09	E 02	2030±0030	3.7±.15
Oct. 14	0555±0003	0539 (0544)	yes	yes	X	N 25	W 71	1030±0030	2.6±.1
Nov. 02(4)	1035±0003	<0950 (1138)	yes~0949	yes		N 16	W 90	Perigee	
Nov. 07(5)	0430±0030	0322 (0345)	yes		no obs.	N 14	E 11	2400±0200	4.0±.1
Nov. 24	1000±0005	0914 (0919)	yes	yes	"	N 13	W 31	1200-1500	2.3±.1
Dec. 30	2010±0020	<1927 (1934)	yes	yes	X	S 14	W 85	(31)0100-0800	2.8±.2
1970									
Jan. 03	MED: P2130±0100	1915 (1917)	yes	yes		N 13	W 16	(04)0900±0200	Small I.(b)
Jan. 28	1330±0005	1022 (1032)	yes	yes	-	S 16	W 26	1900-2100	2.9±.1
Jan. 29	1255±0005	1024 (1029)	yes	yes	-	S 13	W 42	2400±0100	2.3±.1
Jan. 31	1605±0005	1512 (1535)	yes	yes	X	S 23	W 62	2000±0100	2.7±.1
Mar. 06	1330±0030	0926	yes	yes	-	N 09	W 90	storm cond.	--
Mar. 07	1100±0200	1122 (1128)	yes	yes	-	S 14	E 48	storm cond.	--
Mar. 21	MED: P0700±0200	0035 (0053)	yes	yes	X	N 18	E 67	(22)0600±0300	2.5±.1 (a)
Mar. 23	1815±0005	1545 (1548)	yes	yes	X	N 18	W 62	2200±0100	2.9±.1
Mar. 25	1400±0100	1202 (1226)	yes	yes	X	N 14	E 10	(26)0900±0200	4.3±.1
Mar. 29	0115±0005	0010 (0046)	yes	yes	X	N 13	W 37	0900±0300	1.8±.2
Apr. 15	0440±0030	0413 (0419)	yes	yes	X	N 13	W 86	1000±0100	2.4±.2
May 30	0520±0030	0226 (0319)	yes	yes	-	S 08	W 30	2030±0100	4.0±.1
June 02	MED: P0930±0030	0618 (0631)	yes	yes	X	S 08	W 76	storm cond.	--
June 14	1700±0030	1321 (1326)	yes	yes	X	N 21	E 42	2300±0100	2.3±.1

** IMPIV reentered the earth's atmosphere on May 3, 1969; IMPV was launched on June 21, 1969.

TABLE I - CONTINUED

DATE	.5-1.1 MeV ELECTRON ONSET TIME (UT)	SOLAR FLARE ASSOCIATION					20-80 MeV MAX. TIME* (UT)	20-80 MeV SPECTRAL INDEX γ ($\frac{dJ}{dE} \sim -E^{-\gamma}$)
		Hα Time (UT) onset	Max.	X-Rays	Radio cm; Type III	Burst Type II and/or IV	Flare Location	
1970								
June 26	0100±0015	(25)1834	(1839)	yes	yes	--	N 10 E 11	perigee
June 28	MED:P2330±0090	1939	(2007)	yes	yes	X	N 20 E 23	(29)1200-2400 small I(b)
July 06	2200±0003	2135	(2140)	yes	yes	X	N 22 W 90	(07)0230±0100 3.0±.2
July 07	1715±0015	--		yes~1654	yes	X	Reg. 10809~W100	2200±0100 2.4±.1
July 21	0630±0010	0440	(0505)	yes	yes	X	N 08 E 44	1200-1800 4.3±.1
July 23	1845±0005	1831	(1843)	yes	yes	X	N 09 E 09	2300±0100 4.2±.2
Aug. 12	2300±0200	2021	(2036)	yes	yes	X	N 11 E 90	(13)2130±0200 2.5±.2 (a)
Aug. 14	MED:P2100±0100	1604	(1635)	yes	yes	X	N 10 E 75	(15)1500±0100 4.8±.2
Nov. 01	1415±0015	1211	(1247)	yes	yes	X	N 16 W 50	1630±0030 small I(b)
Nov. 05	0430±0005	0308	(0330)	yes	yes	X	S 12 E 36	1600±0200 3.7±.1
Nov. 23	1240±0020	1054	(1102)	yes		-	N 08 W 66	(24)0130±0100 2.2±.2
Dec. 06	MED:P0140±0010	(05)2259	(2325)	yes	yes	X	N 16 W 45	0600-0800 small I(b)
Dec. 12	0300±0100	(11)2205	(2241)	yes	yes	X	N 16 W 02	1700±0200 3.45±.15
1971								
Jan. 14	1052±0008	1045	(1048)	yes	yes		S 09 W 55	1330±0030 2.7±.3
	1136±0008	1121	(1122)	yes	yes	X	" "	
Jan. 24	2340±005	2309	(2316)	yes	yes	X	N 18 W 49	saturated --
Apr. 02	<0030	(01)1300	(1322)	yes	yes	X	S 19 W 12	1130±0030 4.0±.1
Apr. 06	1018±0005	0936	(0944)	yes	yes	no obs.	S 19 W 80	1500-1800 3.0±.2
Apr. 20	2000±0006	1924	(1946)	yes	yes	X	S 06 W 50	2400-2800 3.7±.1
Apr. 21	uncertain (~0800±0100)	0605	(0611)	yes	yes	X	N 18 W 46	Perigee --
Apr. 22	1237±0008	0943	(0947)	yes	yes		N 18 W 61	1500-1900 2.7±.1
May 13	1930±0015	1751	(1758)	yes	yes	X	N 11 W 86	(14)0230±0030 2.7±.2
May 14	1520±0020	1414	(1426)	yes	yes	X	N 04 E 11	2230±0030 3.25±.15
May 16(6)	1300±0003	--		no	yes	IVdK~1236	Reg.11294~W125	1500-2000 3.6±.2
June 29	2345±0015	2235	(2238)	gap	yes	X	N 18 W 22	(30)0600±0100 3.5±.1
Sept 01(7)	2000±0005	--		yes~1930	yes	X	Reg.11482~W120	(02)0500 0900 2.0±.2
Oct. 03	MED:P1513±0015	1330	(1351)	yes	yes	X	N 14 E 14	(04)1000~1600 2.5±.5 (a)

*** The telemetry system of IMPV GSFC Cosmic Ray Experiment was off from 11/15/71 to 2/2/72.

TABLE I - CONTINUED

DATE	.5-1.1 MeV ELECTRON ONSET TIME (UT)	SOLAR FLARE ASSOCIATION					20-80 MeV MAX. TIME* (UT)	20-80 MeV SPECTRAL INDEX γ ($\frac{dJ}{dE} \sim -E^{-\gamma}$)
		Hα Time (UT) onset	Max.	X-Rays	Radio cm; Type III	Burst Type II and/or IV	Flare Location	
1972								
Feb. 22	MED: P0130±0030	0029	(0033)	yes	yes	X	N 03 W 02	0800±0100	3.0±.1
Mar. 05	MED: P1900±0200	0807	(0816)	yes	yes	X		
		1136	(1141)	yes	yes	X	S 07 E 42	Perigee	--
Mar. 11	MED: P0115±0015	0020	(0024)	yes	yes		S 11 W 32	0230±0030	small I(b)
May 28	1452±0008	1310	(1324)	yes	yes	X	N 09 E 30	not identif.	--
June 08(8)	>0600, <1700	--			yes	II~1317	Reg.11895~W110	2100±0100	3.0±.1
June 12	2100±0200	1318	(1334)	yes	yes	X	S 11 E 52	(14)2130±0030	4.5±.1(a)
July 19(9)	0510±0020	--		no	yes	X	Reg.11976~W140	2100±0300	2.6±.1
July 22(9)	0530±0030	--		no		uncertain	Reg.11976~W180	(25)0400-2400	2.5±.4(a)
Aug. 02	0515±0015	0316	(0410)	yes	yes	X	N 14 E 37	2330±0030	3.7±.1
Aug. 03	0230±0030	(02)1958	(2058)	yes	yes	X	N 14 E 29	1900±0200	4.2±.2
Aug. 04	uncertain	0617	(0640)	yes	yes	X	N 14 E 08	Saturated	--
Aug. 07	1540±0005	1449	(1534)	yes	yes	X	N 14 W 37	Saturated	--
Oct. 29	2005±0015	1544	(1747)	yes	yes	X	S 10 E 02	(30)0000±0100	4.0±.2
Oct. 30	0530±0030	(29)2345	(2349)	yes	yes	X	S 09 W 04	2230±0100	4.0±.2
Nov. 25	0903±0005	0820	(0830)	yes	yes	X	S 06 W 44	1300±0100	--
Nov. 28	0400±0010	0355	(0403)	yes	yes	X	S 08 W 80	1100±0100	3.1±.1

(a) The spectral index γ was measured at a time of maximum intensity more than one day after the particle onset time.
(b) The small intensity of those events makes difficult the measurement of the proton spectrum between 20 and 80 MeV since above 30 MeV the galactic component is not negligible compared to the solar components.
(1) This event could not be associated either with an X-ray burst or with a radio burst. However the strong activity of the region 8818 during the passage on the visible disc , and the relative amplitude and onset time respectively on Pioneer 6 and 7 and IMPIV, at different azimuthal positions, makes this region a most probable candidate. It has been also estimated as a probable association by R. E. Gold et al., (1973).
(2) also associated with region 9091 by G. M. Simnett, (1972).
(3) strongly evidenced by radio observations, S. F. Smerd, 1970. Also discussed by McCracken et al., (1971)
(4) Association discussed by C.J. Thomas (1970) also compilation of this event published by D.B. Bucknam and J.V. Lincoln (1971).
(5) Most probable association. The absence of radio burst associated with this flare makes this association uncertain. Also regarded as a possible candidate by Barouch et al. (1971).

FOOTNOTES - CONTINUED:

(6) A type IV radio burst was observed by Boulder and Sagamore Hill observatories. Complementary information on the position provided by the radioheliograph of Nancay (France) (M. Pick, private communication, 1971) shows that the events could be associated with region 11294 which passed the limb two days before the particle onset.

(7) Association discussed by M.A. VanHollebeke , et al., (1972).

(8) The active region 11895 which produced several particle events passed the limb on June 07. Therefore, a flare in this region may be regarded as a good candidate. However, no position measurement of the radio burst has been made.

(9) Spectral observations by the Culgoora observatory (Australia) shows that while there was no position observation at the time of the Type II, the spectra of both radio events (0355.7 UT and 0420 UT) are compatible with behind-the-limb activity (S.F. Smerd, private communication). Furthermore, the region 11957, precursor of the region 11976, producer of the large August solar flares, showed some activity and a very complex magnetic field at its passage on the limb on the 15th (H. Zirin and K. Tanaka, 1972) which may be compatible with strong activity a few days later.

(10) The time profile of this event is reminiscent of some other backside events. In such a case, the region would be the most probable candidate.

TABLE II

Distribution of the Number of Events as a Function of Maximum Particle Intensity

20-80 MeV Proton Maximum Intensity (particles/cm^2 - sec -Sr-MeV)	$>10^{-4} - 10^{-3}$	$>10^{-3} - 10^{-2}$	$>10^{-2} - 10^{-1}$	$>10^{-1} - 10^{0}$	$>10^{0} - 10^{1}$
Number of Detected Events	65	46	32	13	7
Number of Identified Events	40	27	20	13	7

REFERENCES

Altschuler, M.D. and Newkirk, G., Jr.: 1969, Solar Phys. 9, 131.

Axford, W. I.: 1965, Planetary Space Sci. 13, 1301.

Axford, W.I.: 1970, USSR Academy of Sciences Seminar on Cosmic Ray Generation on the Sun, Leningrad.

Barcus, J.R.: 1969, Solar Phys. 8, 186.

Barouch, E., Engelmann, J., Gros, M., Koch, L., and Masse, Pl: 1970, Intercorrelated Satellite Observations Related to Solar Events, ed. C. Manno and D. E. Page, p. 448.

Barouch, E., Gros, M., and Masse, P.: 1971, Solar Phys. 19, 483.

Bostrom, C. O., Williams, D. J., Hagge, D. E., and McDonald, F. B., Solar Geophysical Data, Solar Proton Monitoring Experiment.

Bryant, D. A., Cline, T. L., Desai, U. D., and McDonald, F. B.: 1962, J. Geophys. Res. 67, 4983.

Bryant, D. A., Cline, T. L., Desai, U. D., and McDonald, F. B.: 1965, Astrophys. J. 141, 478.

Bucknam, D. B. and Lincoln, J. V.: 1971, World Data Center A, Report UAG-13, Data on the Solar Proton Event of Nov. 2, 1969, through the Geomagnetic Storm of Nov. 8-10, 1969.

Burlaga, L. F.: 1967, J. Geophys. Res. 72, 4449.

Datlowe, D.: 1971, Solar Phys. 17, 436.

Dilworth, C., Maccagni, D., Perotti, F., Tanzi, E. G., Mercier, J. P., Raviart, A., Treguer, L.,and Gros, M.: 1972, Solar Phys. 23, 487.

Englade, R. C.: 1971, J. Geophys. Res. 76, 768.

Fan, C. Y., Pick, M., Pyle, R., Simpson, J. A. and Smith, D. R.: 1968, J. Geophys. Res. 73, 1555.

Feit, J.: 1973, Solar Phys. 29, 211.

Fisk, L. A. and Axford, W. I.: 1969, Solar Phys. 7, 486.

Freier, P. S. and Webber, W. R.: 1963, J. Geophys. Res. 68, 1605.

Friedman, M. and Hamberger, S. M.: 1969, Solar Phys. 8, 104.

I.A.U., Quarterly Bulletin on Solar Activity, published by the Eidgenös-

sische Sternwarte Zürich, ed. M. Waldmeier.

Gleeson, L.J. and Axford, W.I.: 1968, Astrophys. J. 154, 1011.

Gold, R.E., Nolte, J.T., Roelof, E.C. and Reinhard, R.: 1973, 13th International Cosmic Ray Conf., Denver, Colo., Proc., 2, 1367.

Jones, S.L., Ludwig, G.H., Stilwell, D.E., Trainor, J.H. and Way, S.H.: 1967, IEEE Transactions on Nuclear Science (NASA/Goddard Space Flight Center), Vol. NS-14, p. 56.

Kinsey, J.H.: 1970, Thesis, A Study of Low energy Cosmic Rays at 1 AU, NASA/GSFC X-611-69-396.

Krimigis, S.M. and Verzariu, P.: 1971, J. Geophys. Res. 76, 792.

Lanzerotti, L.J.: 1972, Proc. National Symp. Natural and Manmade Radiation in Space, NASA TM-X-2440, 193.

Lanzerotti, L.J.: 1973, J. Geophys. Res. 78, 3942.

Lin, R.P.: 1970, Solar Phys. 12, 266.

Lin, R.P.: 1974, Space Sci. Rev. 16, 189.

Lupton, J.E. and Stone, E.C.: 1973, J. Geophys. Res. 78, 1007.

McCracken, K.G. and Rao, U.R.: 1970, Space Sci. Rev. 11, 155.

McCracken, K.G., Rao, U.R. and Bukata, R.P.: 1967, J. Geophys. Res. 72, 4293.

McCracken, K.G., Rao, U.R., Bukata, R.P. and Keath, E.P.: 1971, Solar Phys. 18, 100.

McCracken, K.G., Rao, U.R. and Ness, N.F.: 1968, J. Geophys. Res. 73, 4159.

McDonald, F.B. and Fichtel, C.E.: 1974, High Energy Particles and Quanta in Astrophysics (ed. McDonald and Fichtel), Chapter 5.

McDonald, F.B. and Van Hollebeke, M.A.: 1973, Proc. Symp. on High Energy Phenomena on the Sun (ed. R. Ramaty and R.G. Stone), NASA/GSFC X-693-73-193, p. 404.

McKibben, R.B.: 1972, J. Geophys. Res. 77, 3957.

McKibben, R.B.: 1973, J. Geophys. Res. 78, 7184.

Murray, S.S., Stone, E.C. and Vogt, R.E.: 1971, Phys. Rev. Lett. 26, 663.

Palmer, I.D.: 1973, Solar Phys. 30, 235.

Parker, E.N.: 1965, Planetary Space Sci. 13, 9.

Rao, U.R., McCracken, K.G., Allum, F.R., Palmeira, R.A.R., Bariley, W.C. and Palmer, I.: 1971, Solar Phys. 19, 209.

Reid, G.C.: 1964, J. Geophys. Res. 69, 2659.

Reinhard, R. and Roelof, E.C.: 1973, 13th Int. Cosmic Ray Conference, Denver, Colorado, Proc., 2, 1378.

Reinhard, R. and Wibberenz, G.: 13th Int. Cosmic Ray Conference, Denver Colorado, Proc., 2, 1372.

Reinhard, R. and Wibberenz, G.: 1974, to be published in Solar Physics.

Schatzman, E.: 1963, Annales D'Astrophysique 26, 234.

Simnett, G.M.: 1971, Solar Phys. 20, 448.

Simnett, G.M.: 1972, Solar Phys. 22, 189.

Simnett, G.M.: 1974, Space Sci. Rev. 16, 257.

Smerd, S.F.: 1970, Proc. Astron. Soc. Australia, 1, 305.

Solar Geophysical Data, NOAA, U.S. Department of Commerce, Boulder, Colorado, 80302.

Sturrock, P.A.: 1973, IAU Symposium No. 57 on Coronal Disturbances, Australia.

Syrovatsky, S.I.: 1970, Acta Physica Academiae Scientiarum Hungaricae 29, Suppl. 1, 17.

Thomas, C.J.: 1970, Proc. Meeting on Operation PCA 69, AFCRL-70-0625, 15.

Van Hollebeke, M., Wang, J.R. and McDonald, F.B.: 1972, UAG-24, I, 102.

Van Hollebeke, M.A., Wang, J.R., McDonald, F.B.: 1974, Catalogue of Solar Cosmic Ray Events, IMPS IV and V (May 1967-December 1972), NASA/GSFC X-661-74-27.

Wentzel, D.G.: 1965, J. Geophys. Res. 70, 2716.

Zirin, H. and Tanaka, K.: 1973, Bull. American Astron. Soc. 5, 282.

FIGURE CAPTIONS

Figure 1. Distribution of the $\sim$ 125 identified solar events with respect to the heliolongitude of the associated flare. The definition of an event requires that the differential flux of proton $\geq$ 20 MeV exceeds 10^{-4} particles/cm^2- sec -sr-MeV.

Figure 2. Examples of 3 classical particle time histories. The onset times of the .5 - 1.1 MeV electrons are used to identify the associated flare. An arrow or a dashed box at maximum particle intensity indicates the time interval used to determine the spectral index, γ_p, for the 20 - 80 MeV energy range.

Figure 3. Examples of micro-events or complex event time profiles. The same convention applies here as in figure 2. Included on these figures are the .9 - 1.5 MeV and the 6 - 19 MeV protons time histories which help to distinguish the non-velocity dependant effect.

Figure 4. Time histories and spectral determination for the April 20 and April 22, 1971 solar particle events. These are examples for which the spectrum can be determined over the same time interval from 4 to 80 MeV. In the case of the April 22 event, a differential power law in kinetic energy fits the data from 4 to 80 MeV. Note, however, the presence of a knee between 15 and 25 MeV in the case of the April 20 event. There might be an effect of particle anisotropy which was directed out of the ecliptic plane.

Figure 5. The time histories of the 20 - 30 MeV, 30 - 50 MeV and 50 - 80 MeV for four events with fast decay times. The source spectra as derived from each of the individual maximum (dashed diamonds) are shown to be identical to that obtained using a single time interval after the 20 - 80 MeV maximum intensity. This illustrates that over this limited energy range the energy dependence of the interplanetary diffusion coefficient is sufficiently weak.

Figure 6. The spectra of two events at the time of maximum intensity as determined from both OGO V and IMP V are shown for comparison. The IMP V detector points in a direction perpendicular to the ecliptic. OGO V is always looks away from the earth in the ecliptic plan. In April 1971 OGO V was pointingin the direction of the nominal field line, and in November 1969, it was pointing in the direction $\sim 60°$E from the sun-earth line. A small variable anisotropy which might still be present at the time of maximum did not affect the distribution of the particles.

Figure 7. A spectral shape of the form $J = J_0 e^{-p/p_0}$ is shown as a possible alternative for 3 events with different spectral slopes. Whenever a unique spectrum could be determined over an energy range from 10 - 80 MeV, a power law in differential kinetic energy gave a better fit.

Figure 8. 20 differential energy spectra are shown as representatives of the spectra determined for the 90 events included in this

study. The spectral index γ_p and the time of measurement near the maximum particle intensity are shown. These values are also listed in Table I for all events.

Figure 9. Distributions of the spectral index γ_p determined at the time of maximum proton intensity in the 20 - 80 MeV and the 4 - 20 MeV range. These values of γ_p show a Poisson-like distribution with an average of 2.9 for the 20 - 80 MeV range and 2.4 for the 4 - 20 MeV.

Figure 10. Variation of the spectral index γ_p in the 20 - 80 MeV range as a function of the heliolongitude $\lambda_\odot$. The open circles are "long rise time events" with a rise time longer than 24 hours. For these events, it is felt that effects of interplanetary propagation are not negligiable. The dashed contour lines enclose 92% of all the other events. The solid line is a least square fit obtained for them. $\gamma_p\ (\lambda_\odot)$ can be represented approximately by $\gamma_p\ (\lambda_\odot) = 2.7\ [1 + \frac{\Delta\lambda}{2}]$.

Figure 11. Distribution of the number of events as a function of the spectral index γ_p at 20 - 80 MeV and in the preferred longitude range $\lambda_\odot$ = 20 - 80°W.

Figure 12. Variation of the Differenital energy spectral index γ_p in the 4 - 19 MeV range with heliolongitude $\lambda_\odot$. There appears to be no systematic variation.

Figure 13. The difference ΔT_m of the time between onset of 20 - 80 MeV proton and maximum particle intensity is plotted as a function

of the heliolongitude. The solid line is a least square fit through the data. It shows a mimimum at $\sim 50° \pm 30°$ West of the central meridian.

Figure 14. Distribution of the number of events in the 20 - 80 MeV energy range as a function of the rise time T_r for events in the longitude range $\lambda_\odot$ = 20 - 80°W. T_r is the time between maximum particle intensity and the assumed acceleration (i.e. x-ray onset time or the equivalent).

Figure 15 Distribution of the rise time T_r as a function of the spectral index γ_p of 20-80 MeV for events in the longitude range $\lambda_\odot$ = 20° W - 80° W. There is a tendency for a long T_r to be associated with a small γ_p.

Figure 16 Variation of the rise time T_r of 20-80 MeV protons with the spectral index γ_p for all events with T_r < 24 hours. The dashed contour lines are the envelope of the data showing a linear relation of the form $\gamma_p = aT_r + b_1$.

Figure 17 A plot of the number of events per unit of intensity $\Delta N/\Delta I$ as a function of the 40 MeV maximum proton intensity. I is defined as I = dJ/dE in particles/cm^2-sec-sr-MeV The two curves are for all detected events and the identified solar particle events respectively.

Figure 18 Variation of the maximum particle intensity as a function of heliolongitude for ~ 40 MeV protons. The data indicated by open circles are deduced from > 30 MeV and > 60 MeV proton intensity of the APL experiments (Bostrom et al.).

Figure 19 Distribution of the number of events per unit of intensity as a function of the maximum proton intensity at 40 MeV for two heliolongitude ranges: $\lambda_{\odot}$ = 20°W - 60° W and $\lambda_{\odot}$ = 60°E - 20° E. A solid and a dashed line fit the data in those respective longitude ranges with the same slope $\alpha \simeq 1.10 \pm .05$.

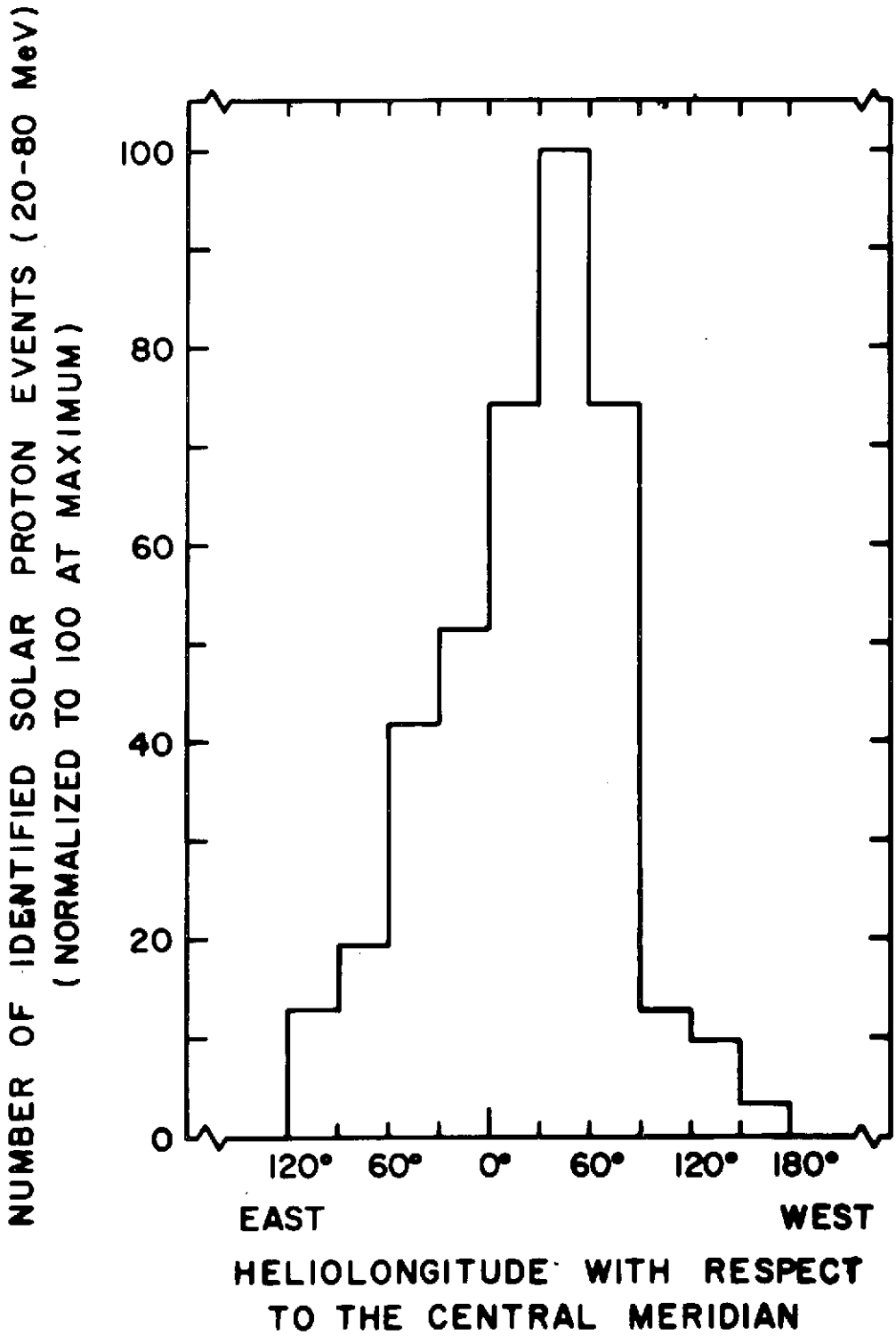
NUMBER OF IDENTIFIED SOLAR PROTON EVENTS (20-80 MeV)
(NORMALIZED TO 100 AT MAXIMUM)
100
80
60
40
20
0
120°
60°
0°
60°
120°
180°
EAST
WEST
HELIOLONGITUDE WITH RESPECT
TO THE CENTRAL MERIDIAN

Figure 1

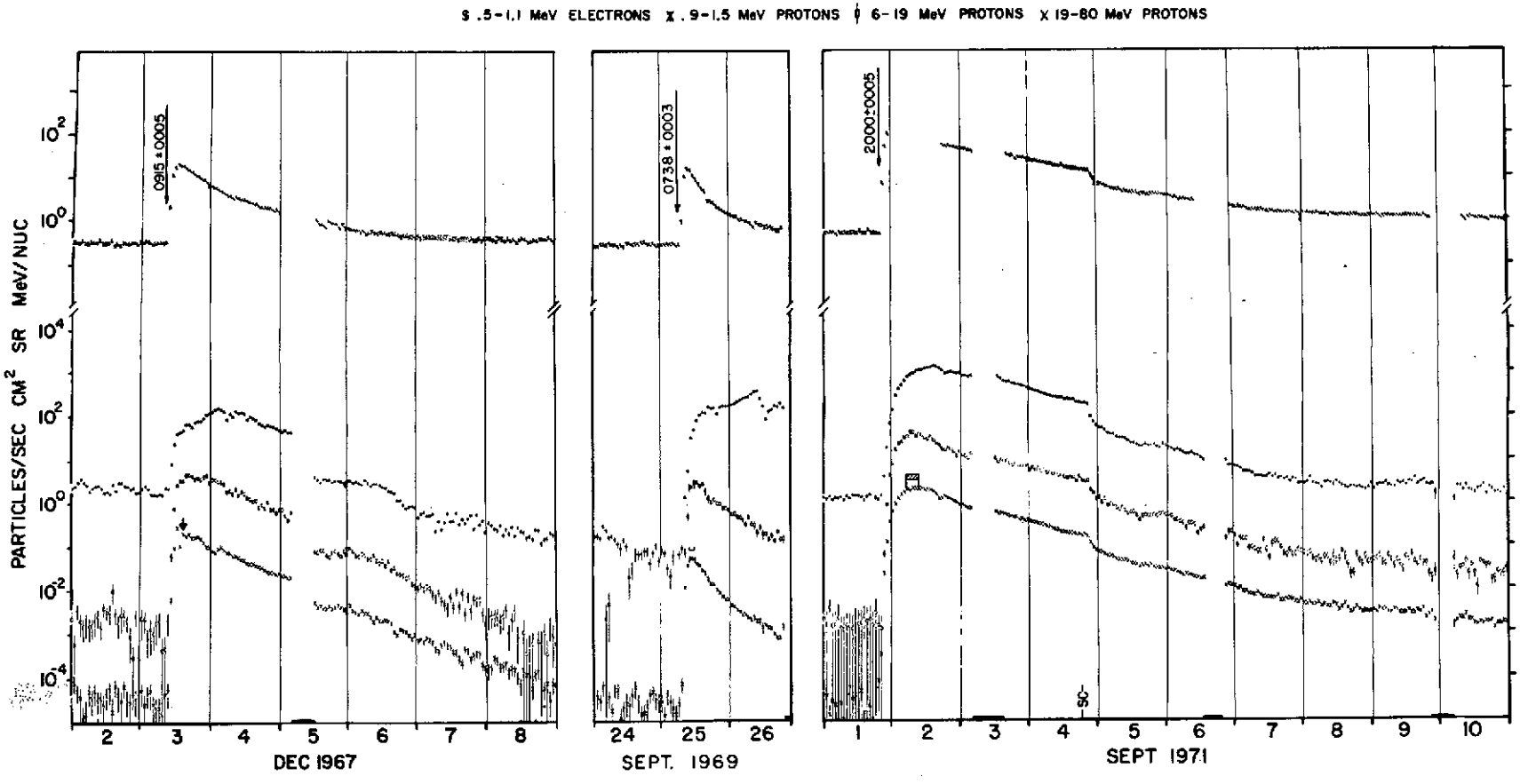
$ .5-1.1 MeV ELECTRONS x .9-1.5 MeV PROTONS ϕ 6-19 MeV PROTONS X 19-80 MeV PROTONS
PARTICLES/SEC CM² SR MeV/NUC
0915 ± 0005
0738 ± 0003
2000±0005
DEC 1967
SEPT. 1969
SEPT 1971

Figure 2

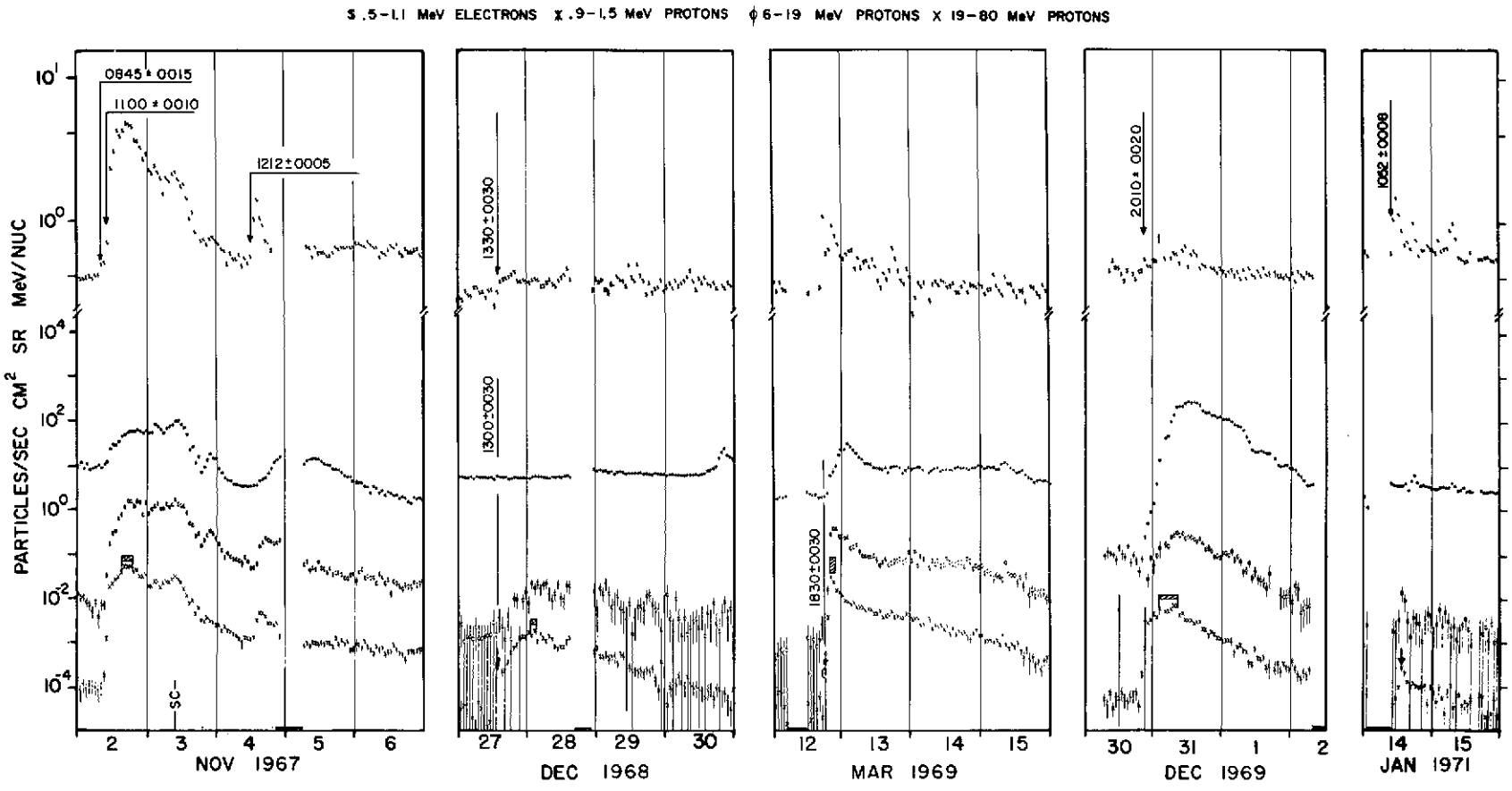
$ .5-1.1 MeV ELECTRONS x .9-1.5 MeV PROTONS ϕ 6-19 MeV PROTONS X 19-80 MeV PROTONS
PARTICLES/SEC CM² SR MeV/NUC
0845±0015
1100±0010
1212±0005
1330±0030
1300±0030
1830±0030
2010±0020
1052±0008
SC
NOV 1967
DEC 1968
MAR 1969
DEC 1969
JAN 1971

Figure 3

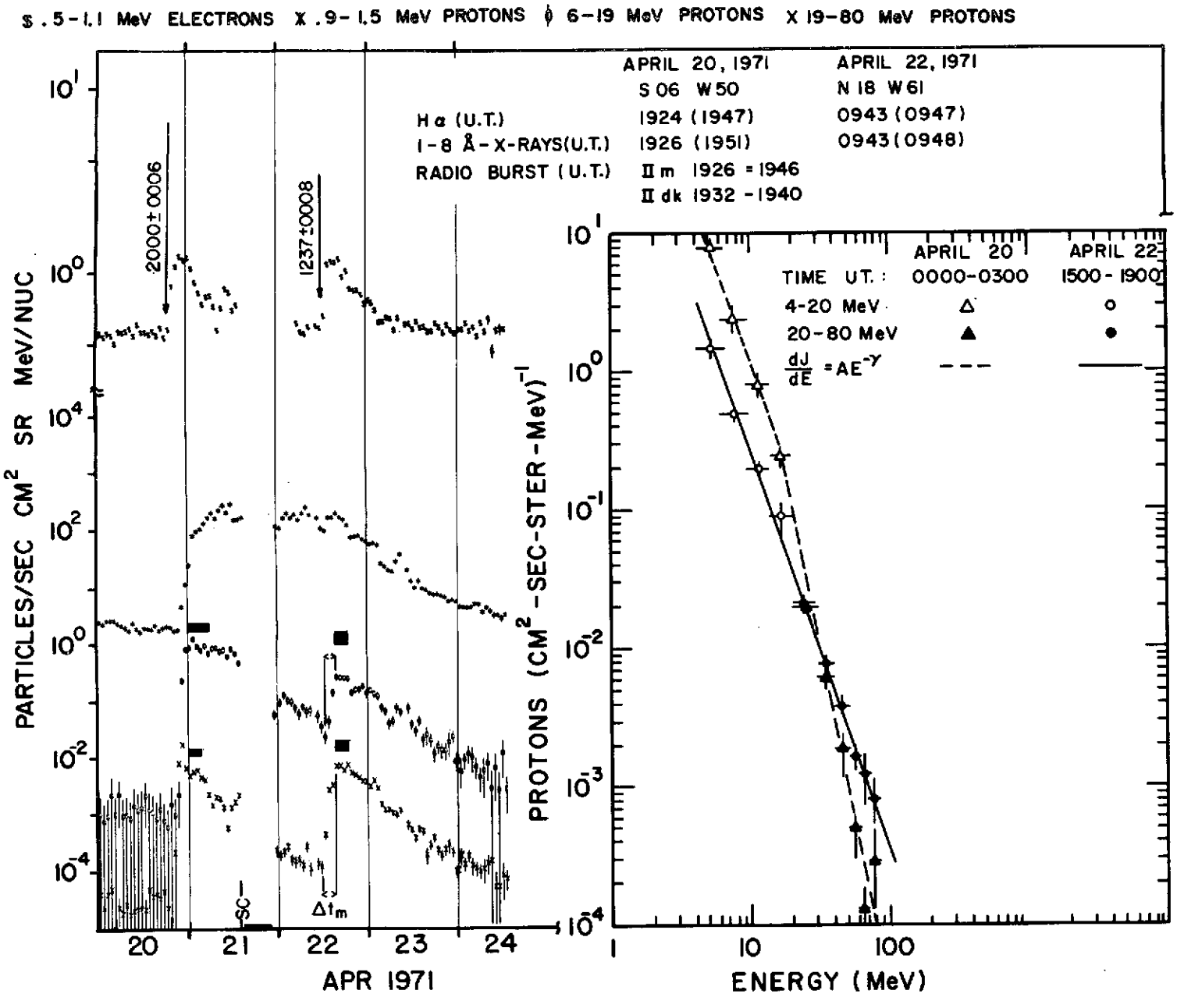
$ .5-1.1 MeV ELECTRONS X .9-1.5 MeV PROTONS ϕ 6-19 MeV PROTONS X 19-80 MeV PROTONS
APRIL 20, 1971
S 06 W50
APRIL 22, 1971
N 18 W61
Hα (U.T.)
1924 (1947)
0943 (0947)
1-8 Å-X-RAYS(U.T.)
1926 (1951)
0943 (0948)
RADIO BURST (U.T.)
II m 1926 - 1946
II dk 1932 - 1940
2000±0006
1237±0008
PARTICLES/SEC CM² SR MeV/NUC
SC
Δtm
20
21
22
23
24
APR 1971
PROTONS (CM²-SEC-STER-MeV)⁻¹
TIME UT.:
APRIL 20
0000-0300
APRIL 22
1500-1900
4-20 MeV
20-80 MeV
dJ/dE = AE^-γ
1
10
100
ENERGY (MeV)

Figure 4

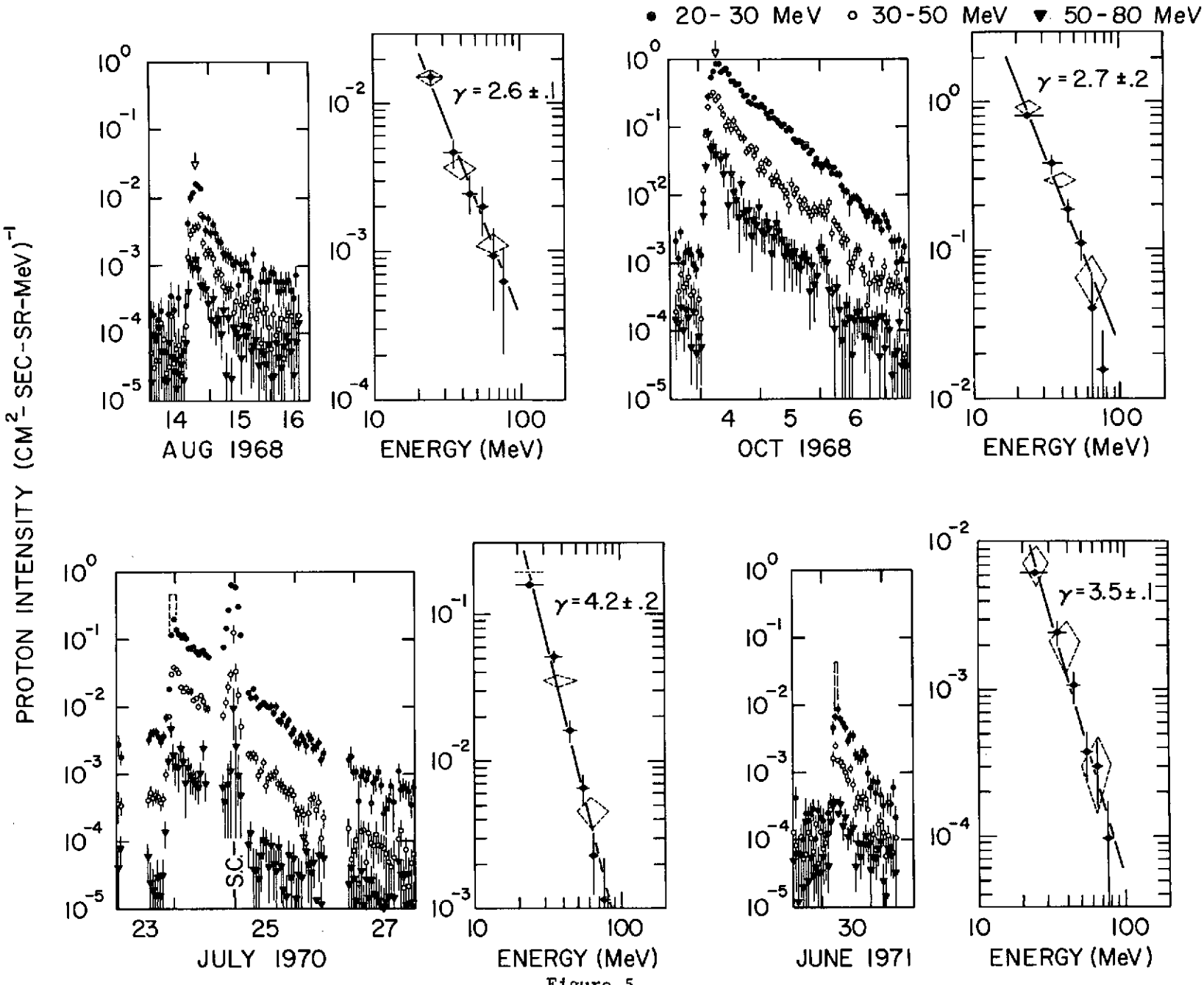
• 20-30 MeV ○ 30-50 MeV ▼ 50-80 MeV
PROTON INTENSITY (CM^2-SEC-SR-MeV)$^{-1}$
AUG 1968
ENERGY (MeV)
γ = 2.6 ± .1
OCT 1968
γ = 2.7 ± .2
JULY 1970
S.C.
γ = 4.2 ± .2
JUNE 1971
γ = 3.5 ± .1

Figure 5

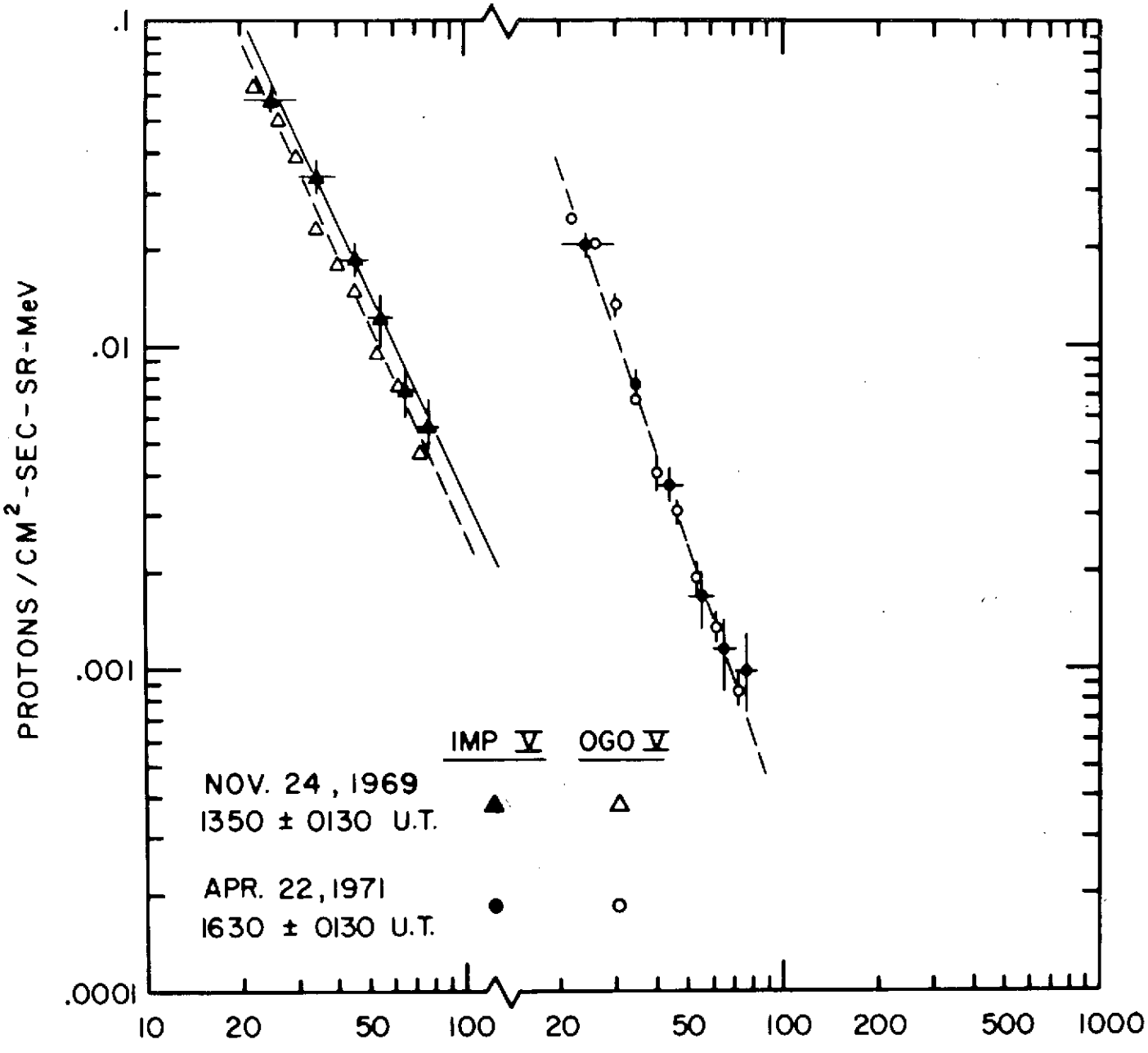
PROTONS / CM^2-SEC-SR-MeV
.1
.01
.001
.0001
10
20
50
100
20
50
100
200
500
1000
IMP V
OGO V
NOV. 24, 1969
1350 ± 0130 U.T.
APR. 22, 1971
1630 ± 0130 U.T.

Figure 6.

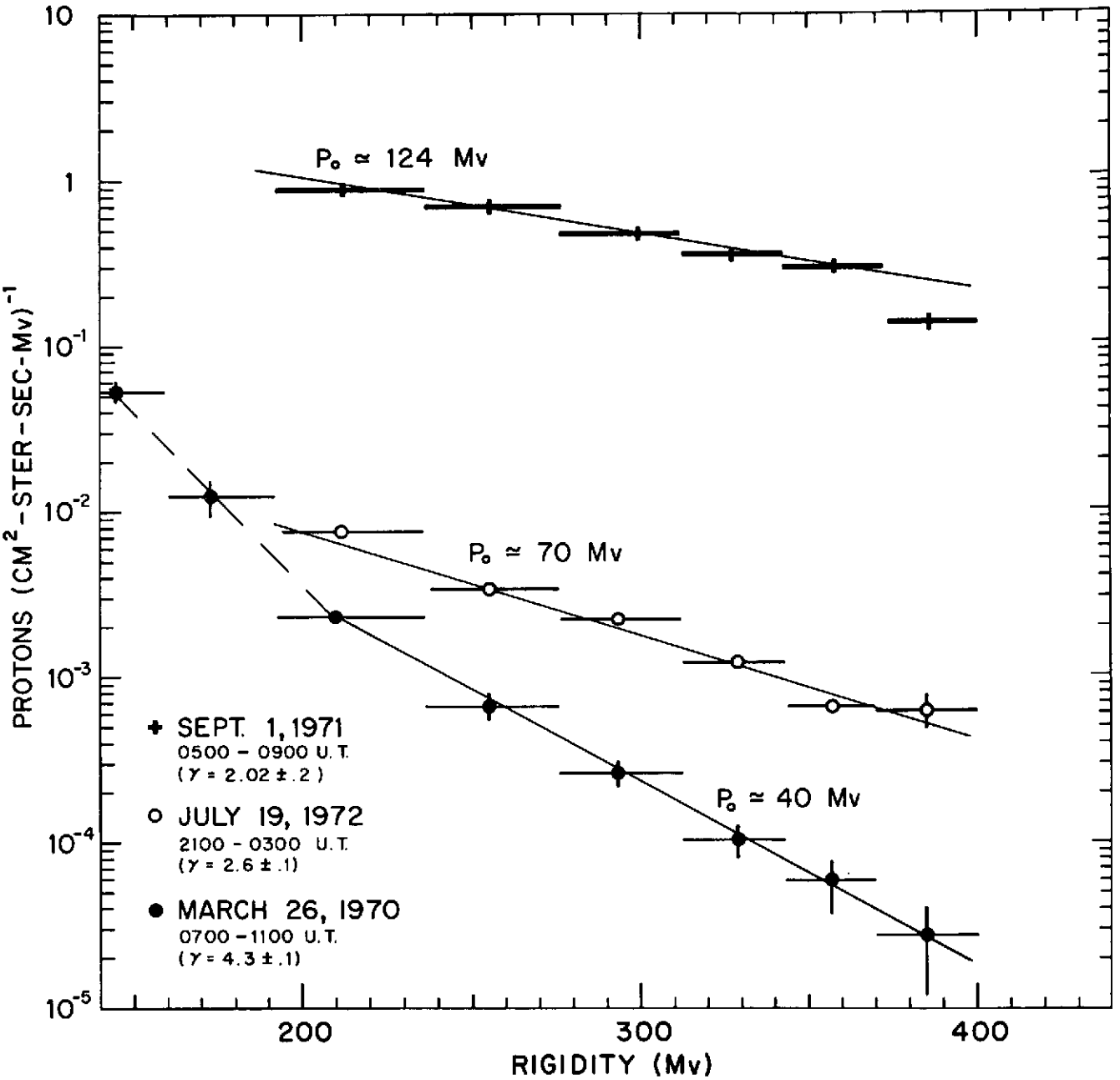
10
1
10^{-1}
10^{-2}
10^{-3}
10^{-4}
10^{-5}
PROTONS (CM^2-STER-SEC-Mv)$^{-1}$
$P_o \simeq 124$ Mv
$P_o \simeq 70$ Mv
$P_o \simeq 40$ Mv
+ SEPT. 1, 1971
0500 - 0900 U.T.
($\gamma = 2.02 \pm .2$)
o JULY 19, 1972
2100 - 0300 U.T.
($\gamma = 2.6 \pm .1$)
● MARCH 26, 1970
0700 - 1100 U.T.
($\gamma = 4.3 \pm .1$)
200
300
400
RIGIDITY (Mv)

Figure 7

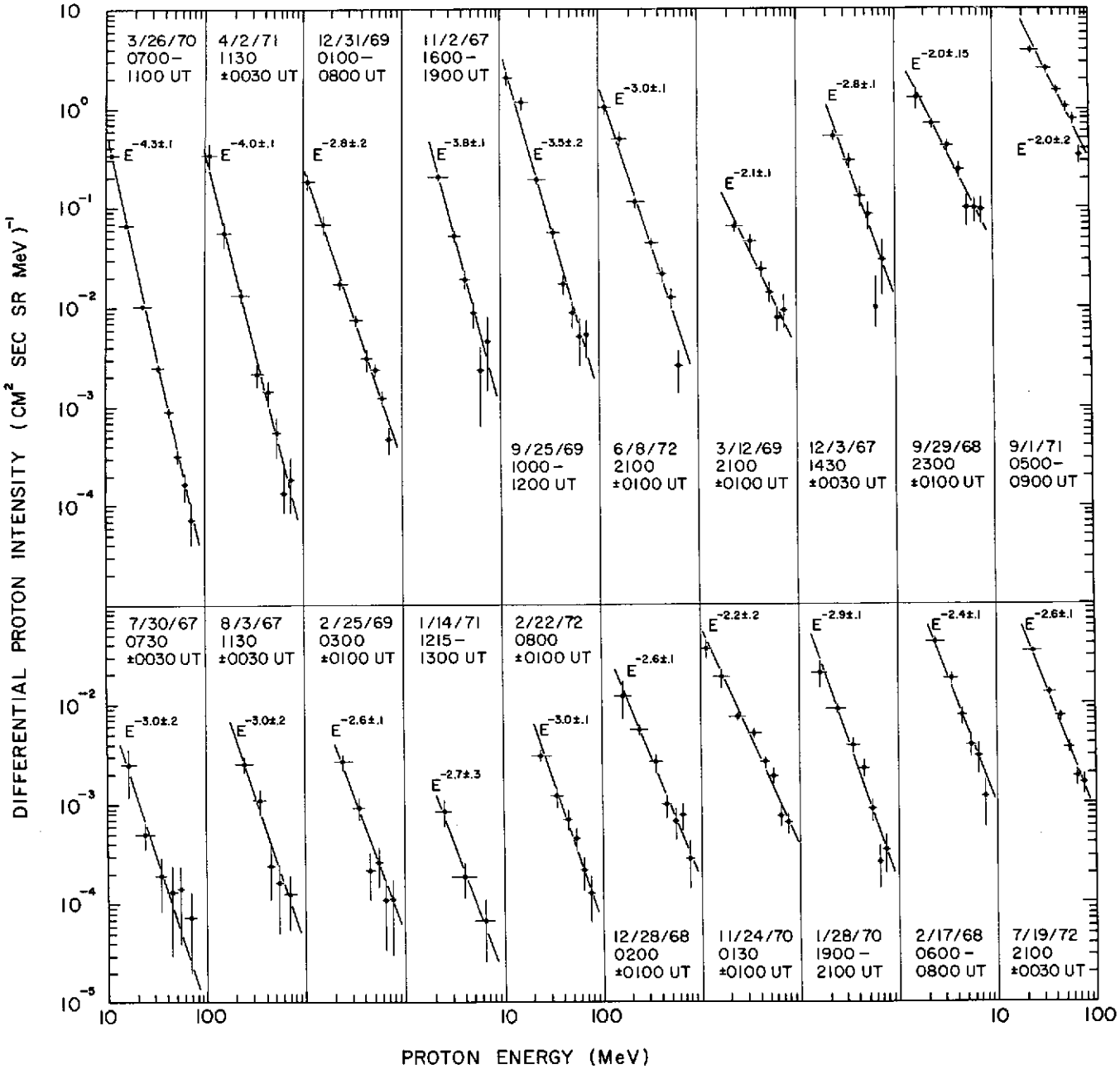
DIFFERENTIAL PROTON INTENSITY (CM² SEC SR MeV)⁻¹
PROTON ENERGY (MeV)
3/26/70 0700– 1100 UT
4/2/71 1130 ±0030 UT
12/31/69 0100– 0800 UT
11/2/67 1600– 1900 UT
9/25/69 1000– 1200 UT
6/8/72 2100 ±0100 UT
3/12/69 2100 ±0100 UT
12/3/67 1430 ±0030 UT
9/29/68 2300 ±0100 UT
9/1/71 0500– 0900 UT
7/30/67 0730 ±0030 UT
8/3/67 1130 ±0030 UT
2/25/69 0300 ±0100 UT
1/14/71 1215– 1300 UT
2/22/72 0800 ±0100 UT
12/28/68 0200 ±0100 UT
11/24/70 0130 ±0100 UT
1/28/70 1900– 2100 UT
2/17/68 0600– 0800 UT
7/19/72 2100 ±0030 UT

Figure 8

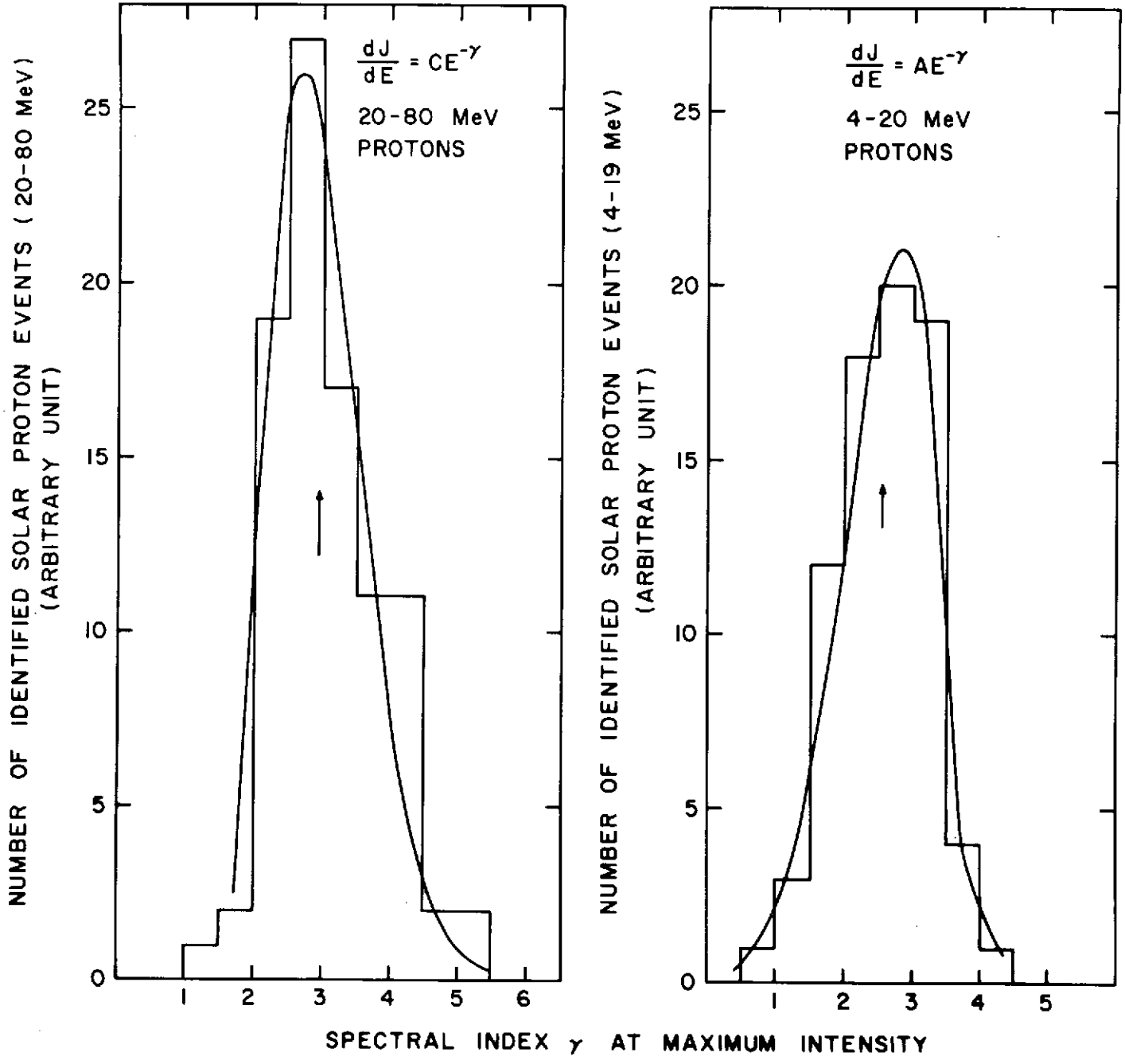
NUMBER OF IDENTIFIED SOLAR PROTON EVENTS (20-80 MeV)
(ARBITRARY UNIT)
dJ/dE = CE^-γ
20-80 MeV
PROTONS
0
5
10
15
20
25
1
2
3
4
5
6
NUMBER OF IDENTIFIED SOLAR PROTON EVENTS (4-19 MeV)
(ARBITRARY UNIT)
dJ/dE = AE^-γ
4-20 MeV
PROTONS
0
5
10
15
20
25
1
2
3
4
5
SPECTRAL INDEX γ AT MAXIMUM INTENSITY

Figure 9

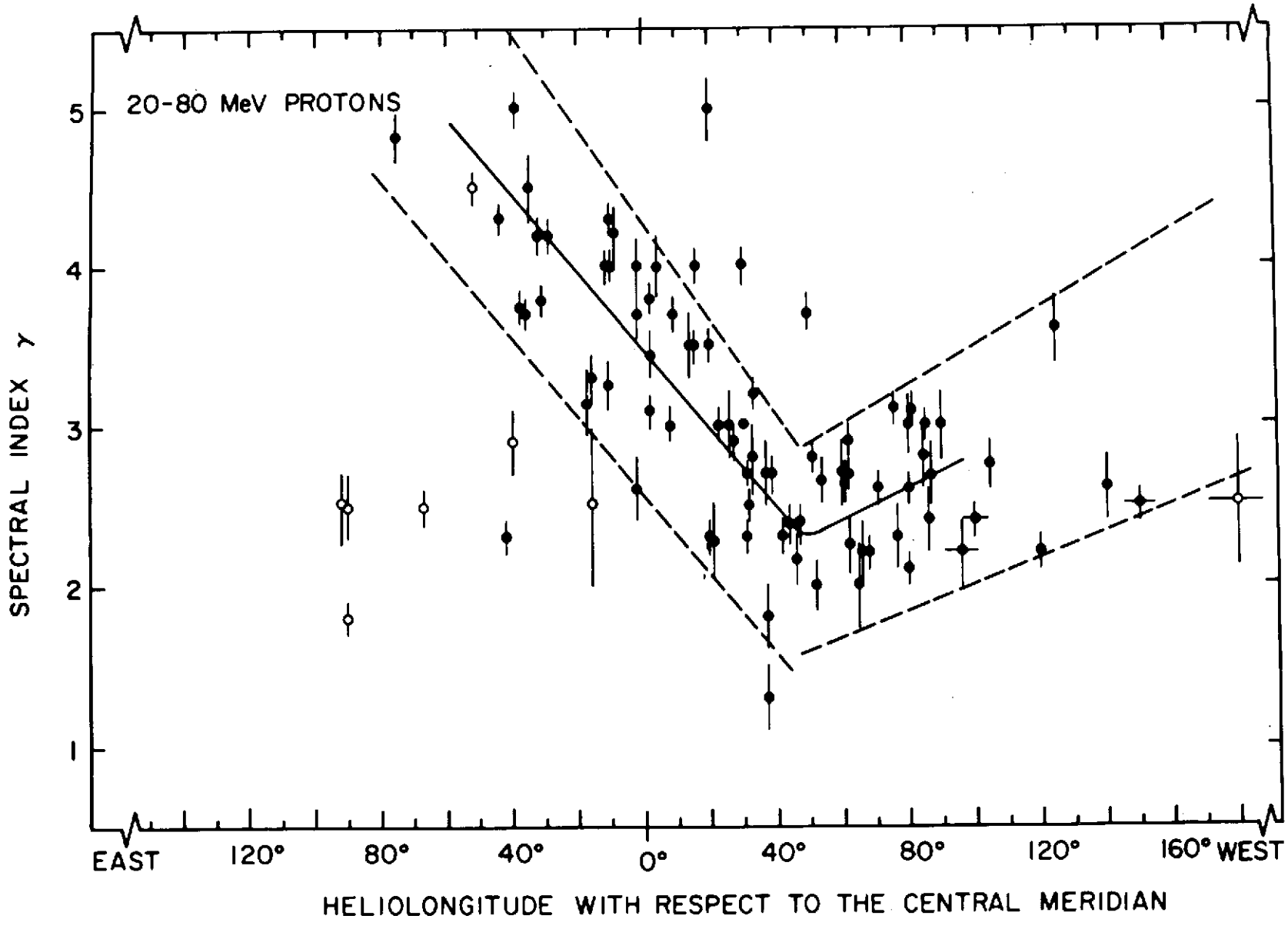
20-80 MeV PROTONS
SPECTRAL INDEX γ
5
4
3
2
1
EAST
120°
80°
40°
0°
40°
80°
120°
160° WEST
HELIOLONGITUDE WITH RESPECT TO THE CENTRAL MERIDIAN

Figure 10.

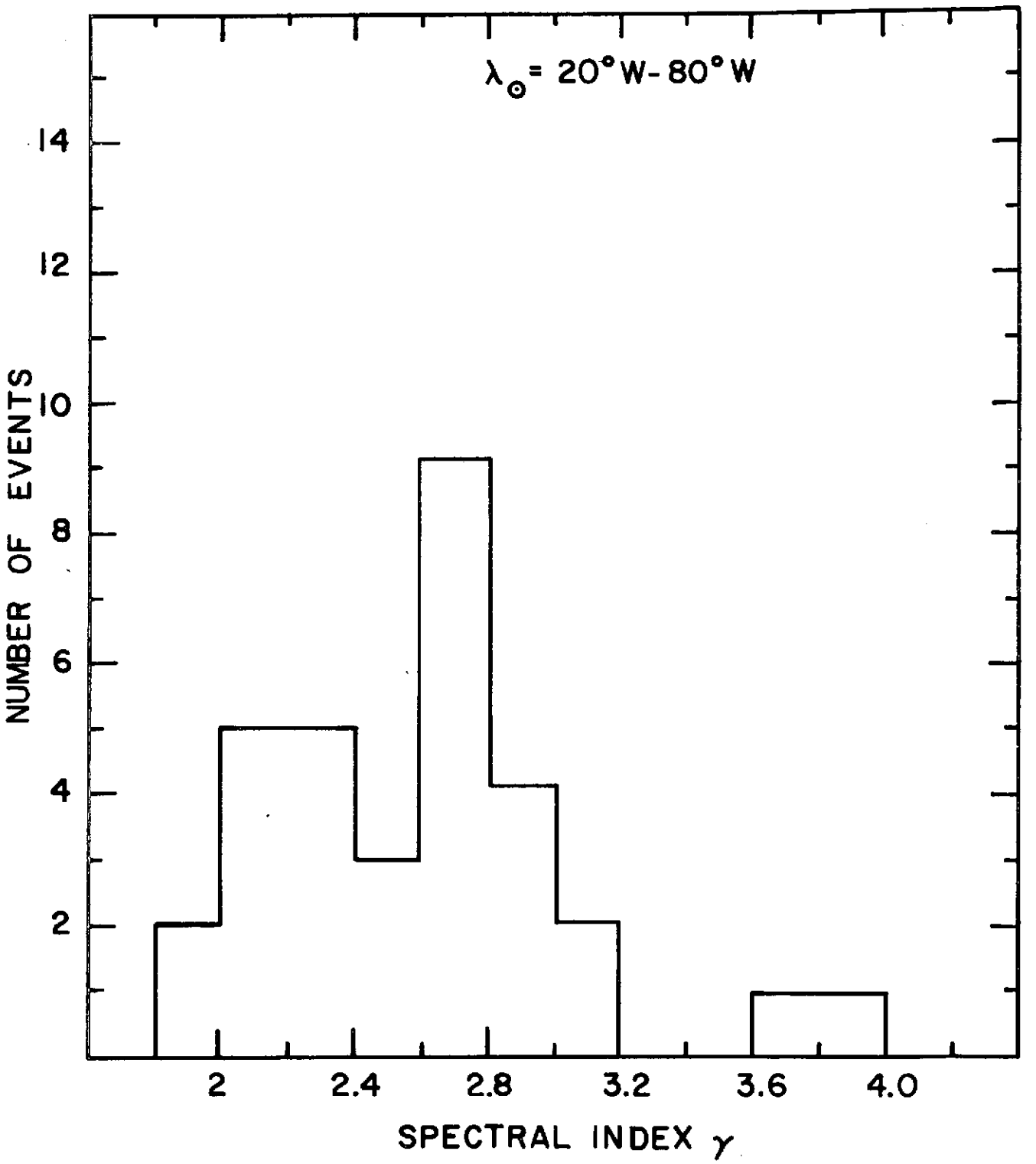
$\lambda_\odot$ = 20°W-80°W
NUMBER OF EVENTS
14
12
10
8
6
4
2
2
2.4
2.8
3.2
3.6
4.0
SPECTRAL INDEX γ

Figure 11

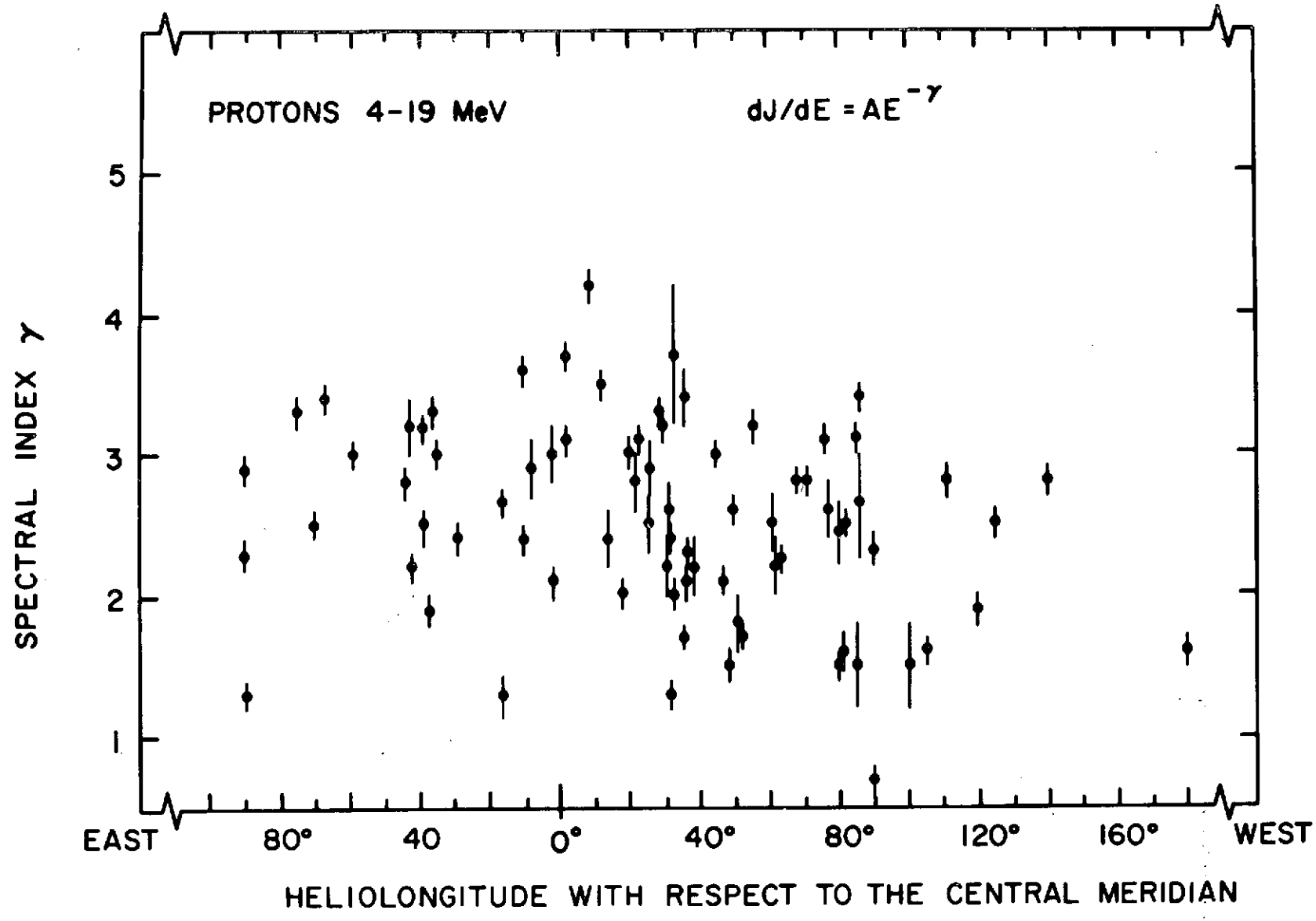
PROTONS 4-19 MeV
dJ/dE = AE^-γ
SPECTRAL INDEX γ
5
4
3
2
1
EAST
80°
40
0°
40°
80°
120°
160°
WEST
HELIOLONGITUDE WITH RESPECT TO THE CENTRAL MERIDIAN

Figure 12

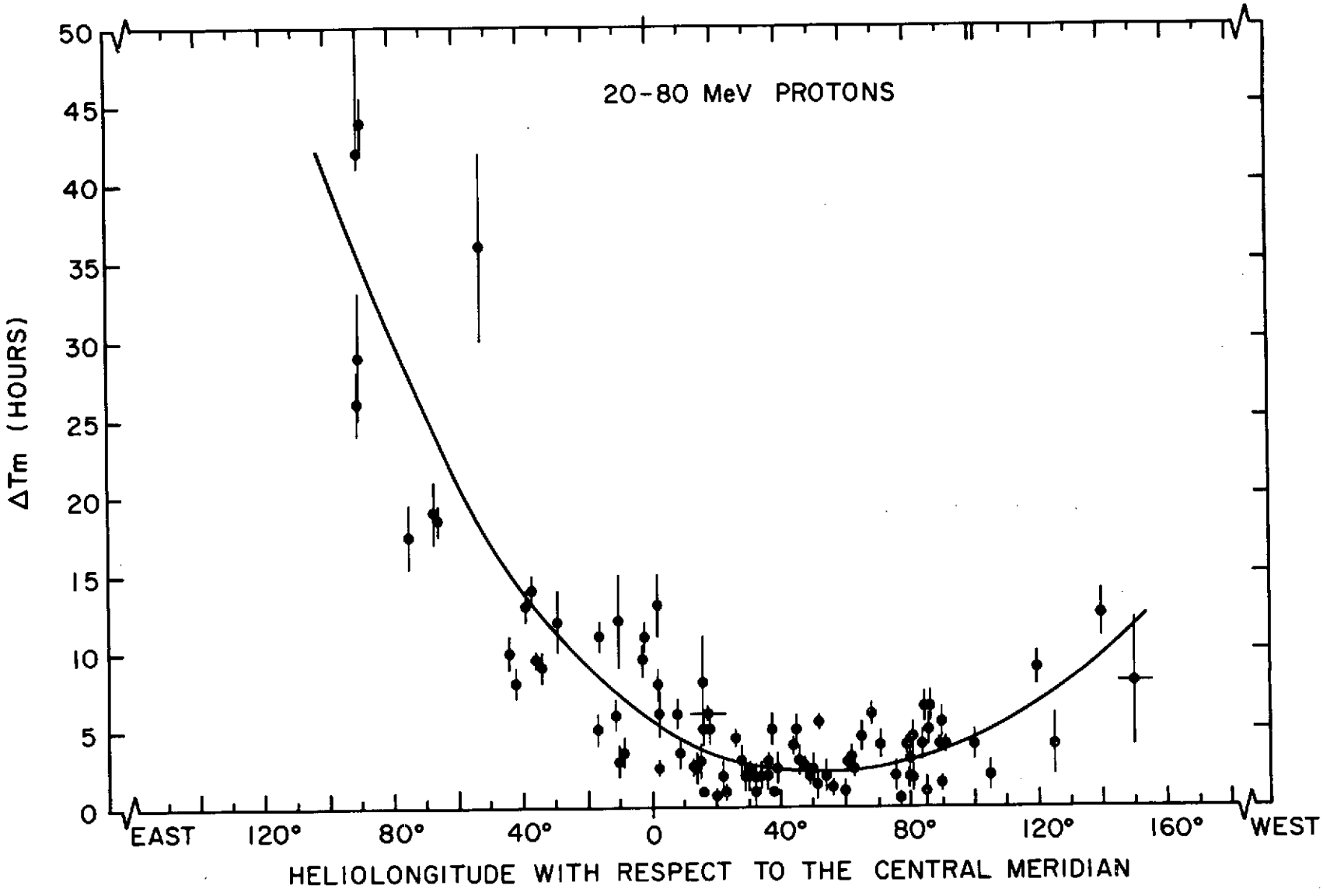
20-80 MeV PROTONS
ΔTm (HOURS)
50
45
40
35
30
25
20
15
10
5
0
EAST
120°
80°
40°
0
40°
80°
120°
160°
WEST
HELIOLONGITUDE WITH RESPECT TO THE CENTRAL MERIDIAN

Figure 13

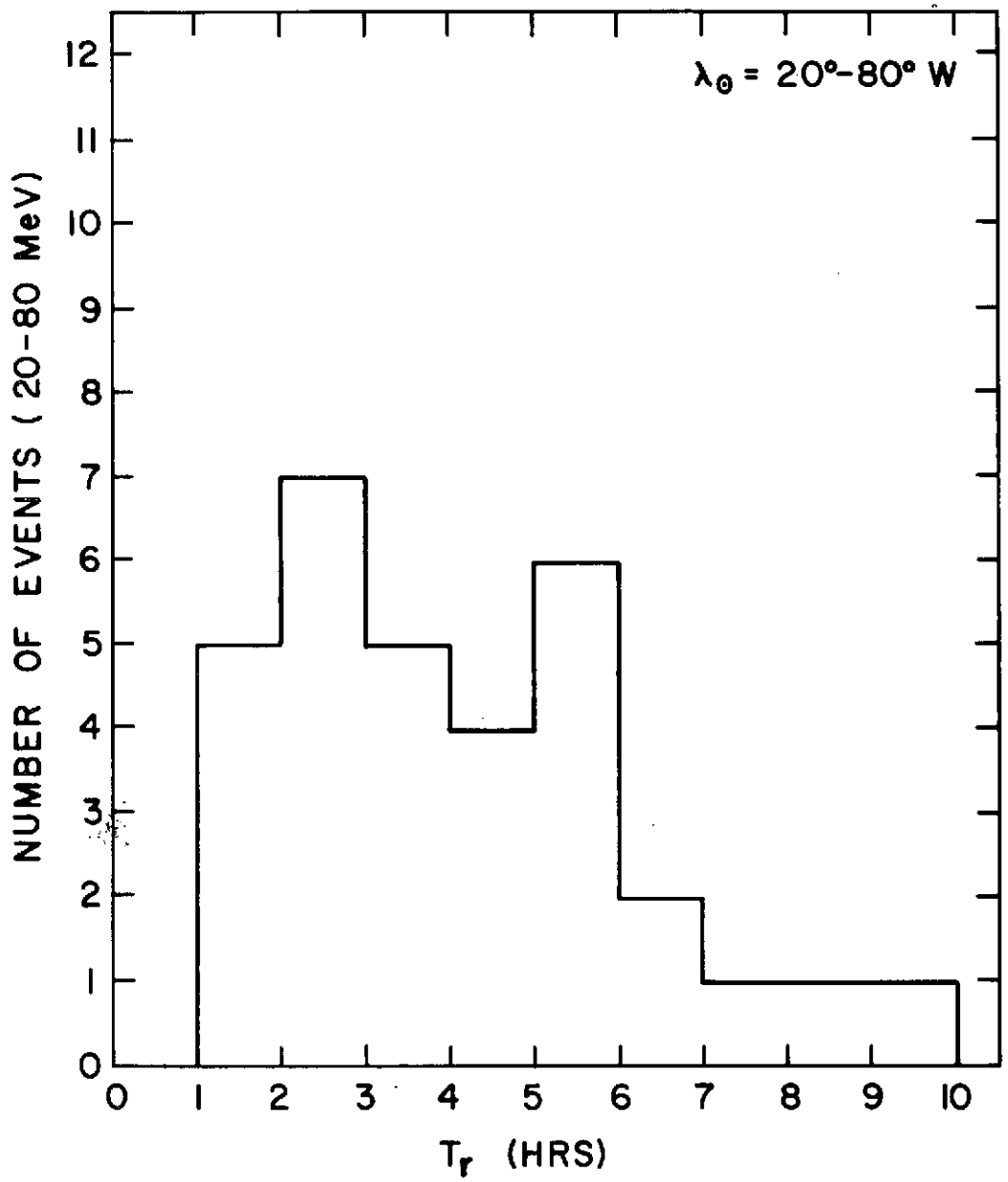
$\lambda_\odot$ = 20°-80° W
NUMBER OF EVENTS (20-80 MeV)
0
1
2
3
4
5
6
7
8
9
10
11
12
0
1
2
3
4
5
6
7
8
9
10
T_r (HRS)

Figure 14

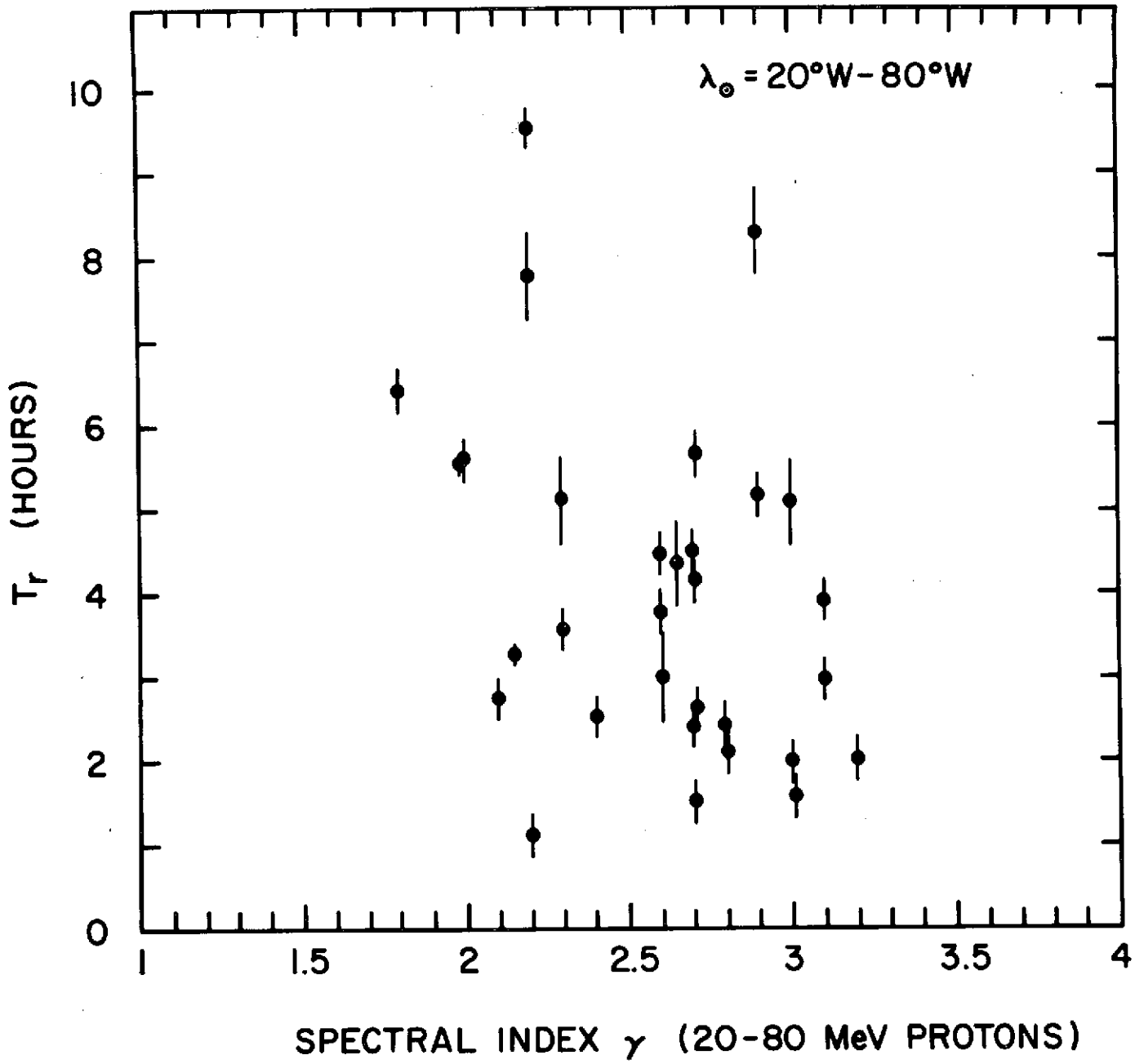
$\lambda_\odot$ = 20°W - 80°W
T_r (HOURS)
0
2
4
6
8
10
1
1.5
2
2.5
3
3.5
4
SPECTRAL INDEX γ (20-80 MeV PROTONS)

Figure 15

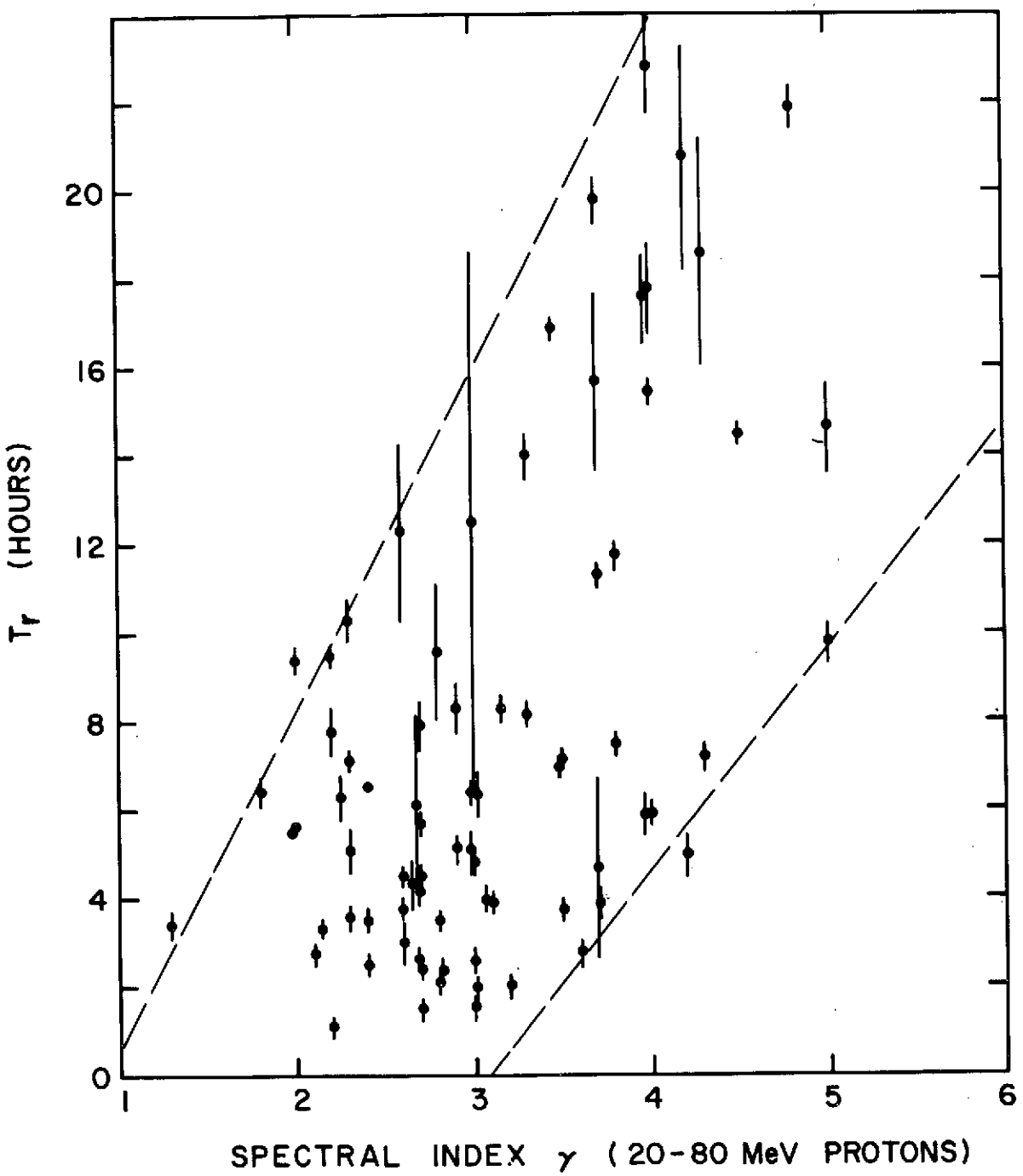
20
16
12
8
4
0
T_r (HOURS)
1
2
3
4
5
6
SPECTRAL INDEX γ (20-80 MeV PROTONS)

Figure 16

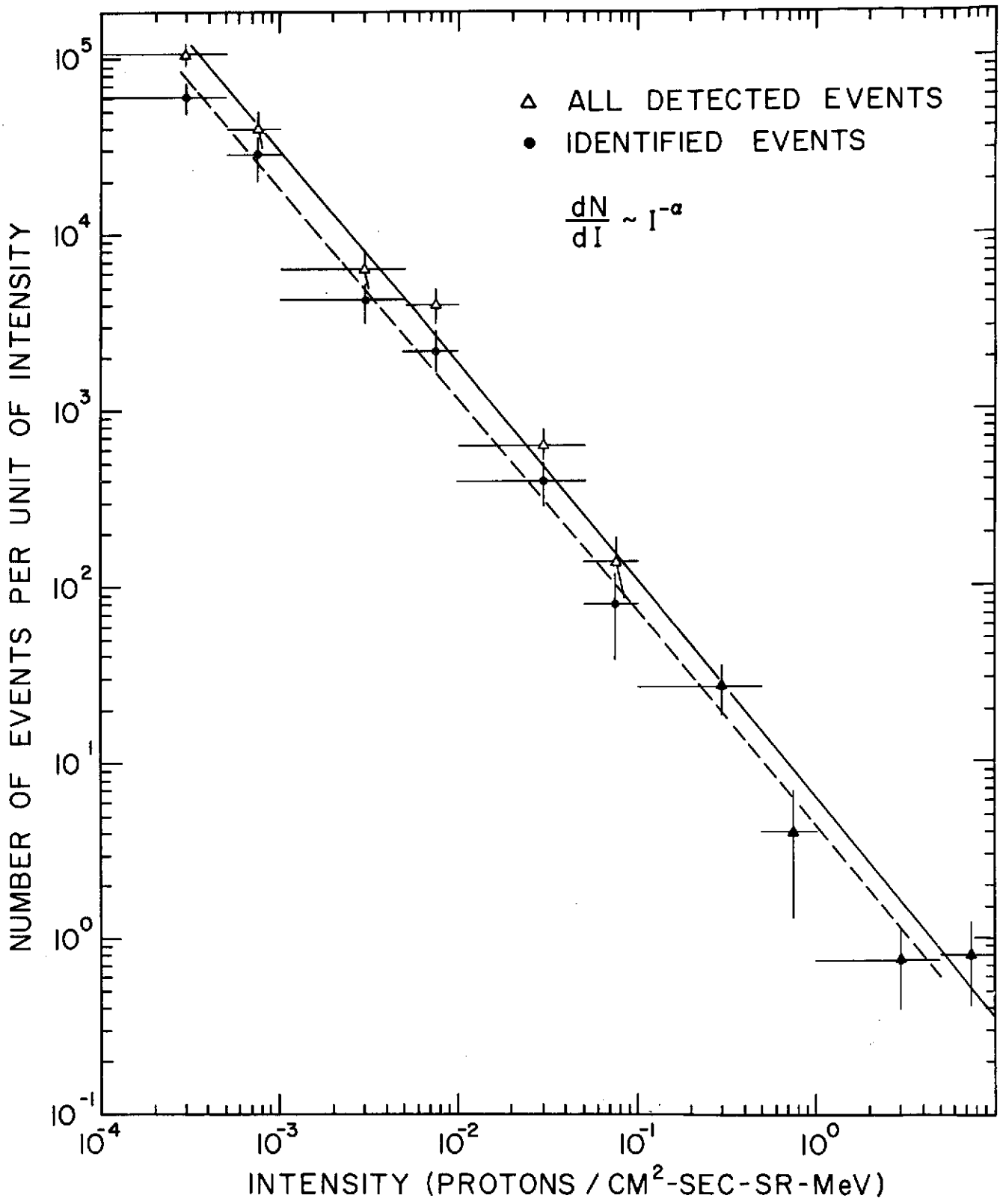
△ ALL DETECTED EVENTS
● IDENTIFIED EVENTS
$\frac{dN}{dI} \sim I^{-\alpha}$
NUMBER OF EVENTS PER UNIT OF INTENSITY
INTENSITY (PROTONS / CM^2-SEC-SR-MeV)
10^5
10^4
10^3
10^2
10^1
10^0
10^{-1}
10^{-4}
10^{-3}
10^{-2}
10^{-1}
10^0

Figure 17

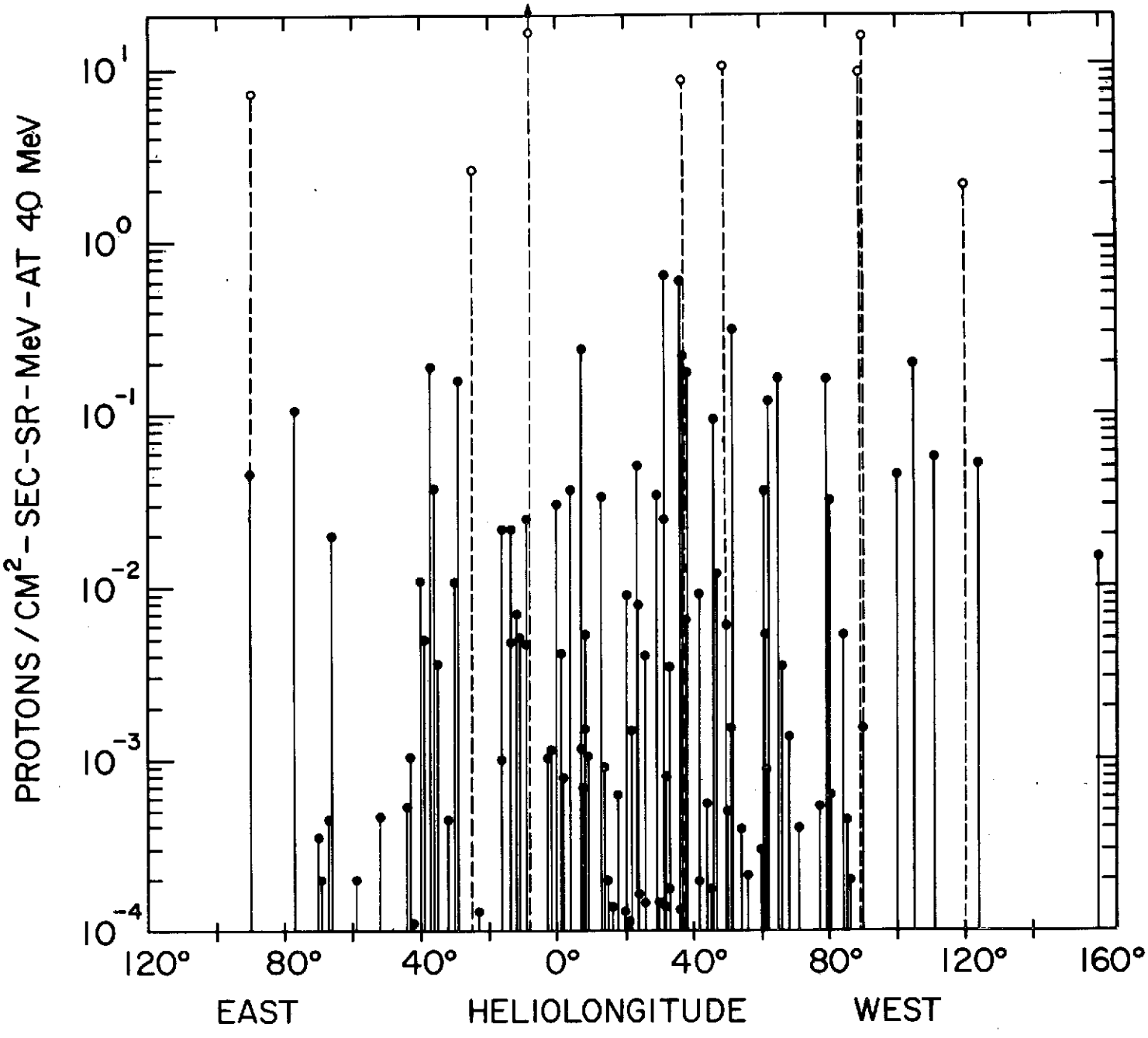
PROTONS / CM^2 - SEC - SR - MeV - AT 40 MeV
10^{1}
10^{0}
10^{-1}
10^{-2}
10^{-3}
10^{-4}
120°
80°
40°
0°
40°
80°
120°
160°
EAST
HELIOLONGITUDE
WEST

Figure 18

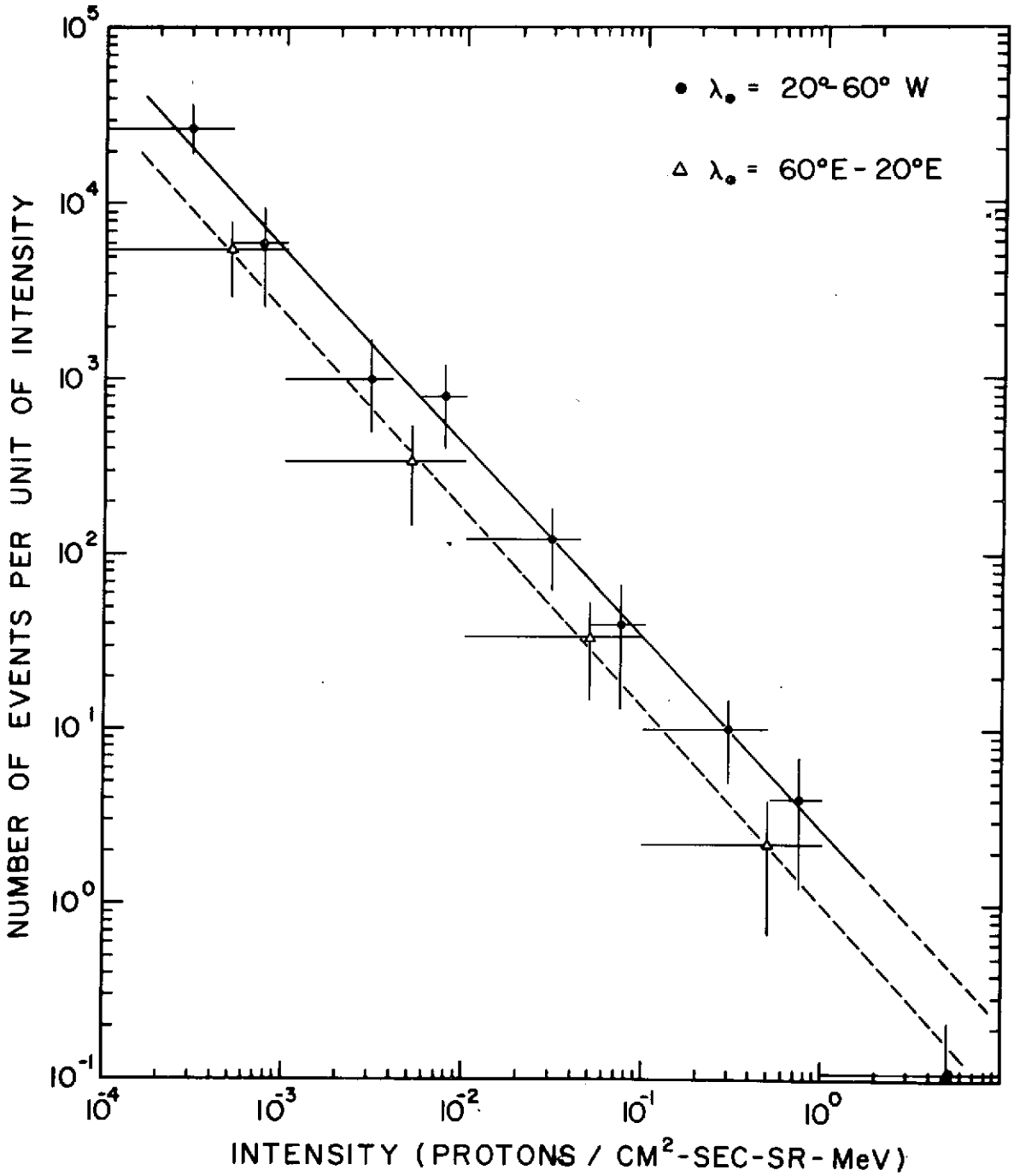
● λ_e = 20°-60° W
△ λ_e = 60°E - 20°E
NUMBER OF EVENTS PER UNIT OF INTENSITY
INTENSITY (PROTONS / CM^2-SEC-SR-MeV)
10^5
10^4
10^3
10^2
10^1
10^0
10^{-1}
10^{-4}
10^{-3}
10^{-2}
10^{-1}
10^0

Figure 19